Unsupervised clustering identifies thermohaline staircases in the Canada Basin of the Arctic Ocean

Mikhail G. Schee[1], Erica Rosenblum[1,2], Jonathan M. Lilly[3], and Nicolas Grisouard[1]

[1]Department of Physics, University of Toronto, Toronto, M5S 1A7, Ontario, Canada, E-mail: mikhail.schee@mail.utoronto.ca
[2]Centre for Earth Observation Science, University of Manitoba, Winnipeg, R3T 2M6, Manitoba, Canada. E-mail: erica.j.rosenblum@gmail.com
[3]Planetary Science Institute, Tucson, 85719, Arizona, USA. E-mail: jmlilly@psi.edu

This paper is a non-peer reviewed preprint submitted to EarthArXiv. This paper has been submitted to the Environmental Data Science journal by Cambridge University press for peer review.

Non-peer reviewed pre-print (2024), **xx**:xx 2–20

APPLICATION PAPER

Unsupervised clustering identifies thermohaline staircases in the Canada Basin of the Arctic Ocean

Mikhail G. Schee[1], Erica Rosenblum[1,2], Jonathan M. Lilly[3] and Nicolas Grisouard[1]

[1]Department of Physics, University of Toronto, Toronto, M5S 1A7, Ontario, Canada, E-mail: mikhail.schee@mail.utoronto.ca.
[2]Centre for Earth Observation Science, University of Manitoba, Winnipeg, R3T 2M6, Manitoba, Canada.
E-mail: erica.j.rosenblum@gmail.com.
[3]Planetary Science Institute, Tucson, 85719, Arizona, USA. E-mail: jmlilly@psi.edu.

Keywords: Arctic Ocean, clustering algorithm, machine learning, thermohaline staircases, ice-tethered profilers

Abstract

Thermohaline staircases are a widespread stratification feature that impact the vertical transport of heat and nutrients and are consistently observed throughout the Canada Basin of the Arctic Ocean. Observations of staircases from the same time period and geographic region form clusters in temperature-salinity (T–S) space. Here, for the first time, we use an automated clustering algorithm called the Hierarchical Density-Based Spatial Clustering of Applications with Noise (HDBSCAN), to detect and connect individual well-mixed staircase layers across profiles from Ice-Tethered Profilers (ITPs). Our application only requires an estimate of the typical layer thickness and expected salinity range of staircases. We compare this method to two previous studies that used different approaches to connect layers, and reproduce several results including the mean lateral density ratio R_L and that the difference in salinity between neighboring layers is a magnitude larger than the salinity variance within a layer. We find that we can accurately and automatically track individual layers in staircases across time and space between different profiles. In evaluating the algorithm's performance, we find evidence of different physical features, namely splitting or merging layers and remnant intrusions. Further, we find a robust dependence of R_L on pressure, whereas previous studies have reported constant R_L. Our results demonstrate that clustering algorithms are an effective and parsimonious method of identifying staircases in ocean profile data.

Impact Statement

Clustering algorithms are unsupervised machine learning methods that are used across many areas of data science. The use of such methods can automate the identification of certain features, thus allowing for analysis of very large datasets. Here, we show that a particular clustering algorithm called HDBSCAN can be used to automatically identify thermohaline staircases in hydrographic profiles from the Arctic Ocean. Compared to previous detection methods, HDBSCAN has the advantages of requiring minimal prior knowledge and of automatically connecting individual staircase "steps" across different hydrographic profiles. We expect that this method could be applied to many similar datasets, offering a straightforward way to identify and track layers in thermohaline staircases across the world's oceans.

1. Introduction

Thermohaline staircases, formed by differential diffusion rates of heat and salt, appear as a series of vertically well-mixed horizontal layers each separated by thin, strongly stratified interfaces. These structures have been observed throughout the world's oceans [47] as well as in saline lakes [28], while related double-diffusive staircases are thought to occur in gas giants such as Jupiter and Saturn [1, 33]. In particular, they are well known to occur in the Arctic Ocean [44, 17, 22]. Around 250 to 800 meters

below the surface of the Arctic Ocean, there is a layer of water originating from the Atlantic, which is warmer and saltier than the topmost layer that is in contact with the sea ice above [44]. The core of the Atlantic Water (AW) is defined as the maximum subsurface temperature and is generally at a depth of 400 meters. Above this depth, in a region in which both temperature and salinity increase downwards, lie the Lower Halocline Waters (LHW) where the staircases are found [17].

Two thirds of the world's oceans are *alpha* oceans which are stratified by temperature, with the warmest waters at the surface and colder waters at depth [42]. This is in contrast to the 15% that are *beta* oceans, the only regions where sea ice can form over deep water, such as the Arctic which are primarily stratified by salinity, and therefore the warm, salty AW is stable at depth [4]. The remaining oceans are called "transition zone oceans" [42]. Historically, the density stratification above the AW core has been strong enough to insulate surface waters from the warmth at depth [40]. However, the lower sections of Arctic staircases have been disappearing in recent years [22], indicating changes to this stratification. If such changes were to continue and eventually allow the heat in the AW to reach the surface, it is estimated that all Arctic sea ice would melt within five years [46]. Indeed, Arctic sea ice is steadily disappearing [6] and exposure to heat from below, in addition to the warming atmosphere above, would accelerate this decline [46]. Given their potential role in modulating the Arctic climate, it is important to be able to accurately identify thermohaline staircases in observations.

The first recorded observation of thermohaline staircases in the Arctic Ocean was made in 1969 at Ice Island T-3 [25]. This iceberg, located somewhat northeast of the Canada Basin (often defined as 72–84°N, 130–155°W, see e.g. Peralta-Ferriz and Woodgate [32]) was the site of dozens of hydrographic profiles that contain clearly visible staircases [26, 27, 24]. Subsequent observations have consistently indicated the presence of staircases in the Canada Basin, including from data collected during the Arctic Internal Wave Experiment (AIWEX) [29, 30, 31] and the Surface Heat Budget of the Arctic (SHEBA) experiment [38]. The frequency of such observations increased dramatically in 2004, when the introduction of autonomous Ice-Tethered Profilers made possible the continuous, year-round sampling of the Arctic Ocean water column [45].

Although many early studies identified staircases by visual inspection, the recent increase in available data has spurred researchers to turn to algorithmic approaches. We find these approaches often have two distinct steps: the detection of data points that fall within some well-mixed layer (henceforth for brevity simply "layer") and the connection of these points to those in other profiles that are within the same layer. Timmermans et al. [44] defined a point in a hydrographic profile to be detected within a layer when the local vertical potential temperature gradient $\partial\theta/\partial z$ is below $0.005°\mathrm{C\,m^{-1}}$, roughly an order of magnitude smaller than the overall gradient for a typical profile. They then sorted these different points into different layers to connect across profiles, although the manner in which this was accomplished does not appear to be specified in the paper. Shibley et al. [40] extended the automated detection method of Timmermans et al. [44] by including two additional conditions: (1) For each experiment, they manually determined different threshold values on both $\partial\theta/\partial z$ and on the temperature difference between neighboring points and (2) after then running the detection method, those authors only considered staircases that consisted of at least three layers. Van der Boog et al. [48] developed a similar staircase detection algorithm, but chose threshold values of vertical density gradients that were expected to be applicable to staircases in all of the world's oceans, not just the Arctic. Specifically, they set a vertical gradient threshold of $\partial\sigma_1/\partial p \leq 0.0005\ \mathrm{kg\,m^{-3}\,dbar^{-1}}$ where σ_1 is the density anomaly referenced to 1000. Then, from the subset of data that meets that condition, only mixed layers with a maximum variation of density anomaly of $0.005\ \mathrm{kg\ m^{-3}}$ or less, and whose neighboring interfaces had thicknesses of 30 dbar or less, were considered. However, neither van der Boog et al. [48] nor Shibley et al. [40] connect any layers between different profiles. Lu et al. [17] defined the intersections between layers and interfaces as locations where the difference in the potential temperature gradient between two neighboring points is greater than $0.003\ °\mathrm{C\ m^{-1}}$, then disregarded the points within the interfaces. With the layer points that remained, those authors then made cross-profile connections, following the work of Padman and Dillon [30] and used valleys in histograms of salinity to guide their choice of boundaries between layers, some of which were manually adjusted.

All of these techniques first detect a subset of the data points that are likely within layers based upon vertical gradient thresholds. This approach requires both sufficient knowledge of the staircases properties in order to select appropriate thresholds, as well as data with sufficient vertical resolution to accurately estimate the gradients. Only Lu et al. [17] document a connection algorithm and it is one which, after its completion, still requires some amount of manual intervention to produce a final dataset of staircase layers. A commonality of all of these approaches is that they are purpose-built for the task of detecting staircases in specific contexts. These factors motivate the search for a more general approach to connecting thermohaline layers across different profiles which could offer advantages such as greater scalability and applicability, more ready reproducibility, and perhaps superior performance, all of which would accelerate the pace of research on these important structures.

Many studies, notably Timmermans et al. [44], have observed that a collection of profiles that includes well-mixed layers, such as density staircases, is associated with clustered patterns when plotted in temperature-salinity (T–S) space [37, 45, 51, 2]. These patterns occur where a staircase is present because all data points within a particular layer have approximately the same temperature and salinity values as other observations from the same layer, regardless of their vertical position within the layer. This fact suggests that staircases could be detected by directly identifying clusters in T–S space. Clustering algorithms are a type of unsupervised machine learning, and have been previously used in a variety of different oceanographic applications [41]. Examples include grouping observations from freely-drifting instruments in the Nordic Seas [14], studying surface wave variability in the North Atlantic [8], classifying the heat content of hydrographic profiles [19], resolving trapping in mesoscale eddies [18], defining spatial regions for Southern Ocean temperature profiles [12], detecting ENSO events [11], finding hot spots for mixing in the Southern Ocean [36], and identifying shifts in the North Atlantic circulation [7]. However, to our knowledge, they have never before been used to identify thermohaline staircases.

Here, we apply a method based on the Hierarchical Density-Based Spatial Clustering of Applications with Noise or HDBSCAN algorithm [3] to both detect and connect thermohaline staircases across Arctic hydrographic profiles. This method has several advantages. It detects and automatically connects staircase layers across large hydrographic datasets in one step. In the past, HDBSCAN has been successfully applied to datasets with a number of points that were an order of magnitude larger than in this study, suggesting the application we present here could be scaled to accommodate more data [16]. Also, it does not consider profiles individually and therefore does not require that each profile have fine vertical resolution. Our implementation of this algorithm does require knowledge of the typical layer thickness and the expected global salinity range of the staircase; however, as we will show, this is a more flexible requirement compared to determining threshold gradients. Most importantly, it exhibits excellent performance producing a final, connected dataset of layers to which no subsequent adjustments need to be made, and is thus suitable for application to datasets with a large number of points as well as being more easily reproducible. The purpose of this paper is to present this method, and so we will note possible implications of our results but will not explore them in great detail.

The structure of this paper is as follows. First, in Section 2, we introduce and explain our choice of the datasets used in our analysis. In Section 3, we introduce HDBSCAN and describe how we use it to identify staircases and how we choose the input parameters. Then, in Section 4, we apply this method to data from two different Ice-Tethered Profiler experiments, focusing on results that reproduce those from the studies of Timmermans et al. [44] and Lu et al. [17], hereafter denoted as T08 and L22, respectively. Finally, in Section 5, we use the comparison between our results and those of T08 and L22 to evaluate the performance of the clustering algorithm and give recommendations on when and how it can be best used to identify staircases.

2. Data

Ice-Tethered Profilers (ITPs) are automated, vertically profiling instruments that are connected via a wire cable to a surface buoy on an ice floe [45]. The wire extends from the surface, through the ice,

Table 1. *Details of the Ice-Tethered Profilers (ITPs) used in this study.*

ITP	Start Date	Days in Operation	Starting Position	Along-path Distance	Longest Span[1]	Total Profiles	Up-going Profiles
2	2004/8/19	40	77° 10.4'N, 141° 13.0'W	390 km	191 km	242	121
3	2005/8/23	382	77° 36.1'N, 142° 11.8'W	2541 km	441 km	1531	766

[1]The maximum distance between any two, not necessarily consecutive, profiles

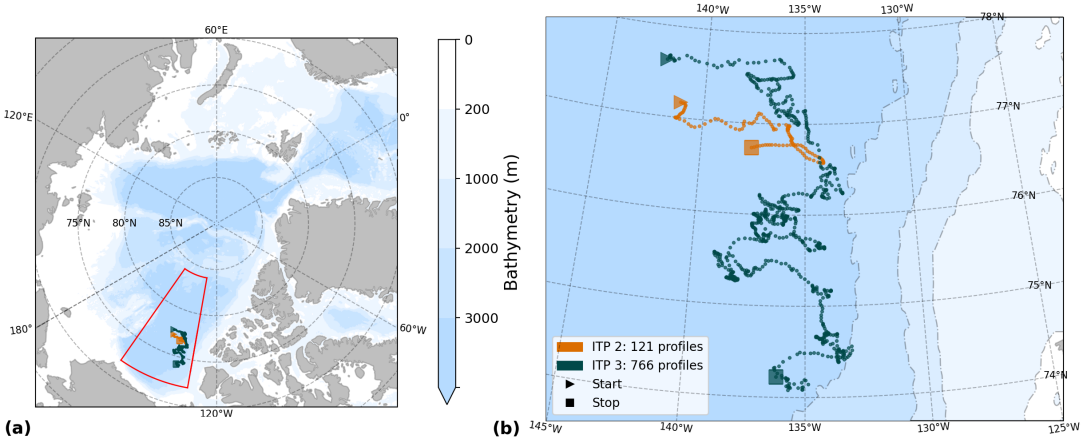

Figure 1. *A map showing the locations of all profiles used from ITPs 2 and 3, showing the whole Arctic in (a) and a zoomed-in view in (b). The red box designates the Canada Basin as defined by Peralta-Ferriz and Woodgate [32].*

down to depths of 500–800 m. The profiler travels up and down the wire roughly two to three times a day collecting high-resolution (~25 cm) measurements of salinity, temperature, and pressure with a salinity precision of ±0.005 g / kg and a temperature precision of ±0.001 ° C [44, 40, 2]. Each traverse, alternating up or down, is recorded as a separate profile.

In this paper, data from two different ITP experiments, ITP2 and ITP3, are analyzed; see Table 1 for a summary. Because the measuring instruments are located at the top of the profiler, we use only the up-going profiles in order to avoid the known distortion caused by the wake of the profiling unit in the down-going profiles [40]. Figure 1 shows the locations of all up-going profiles for each of the two ITP experiments. We choose to analyze ITP2 and ITP3 in particular in order to reproduce several results of T08 and L22, respectively.

At this point we note some choices in the study relative to those of T08 and L22. Here we choose to work with pressure, a directly measured quantity, while both of those studies use depth, which is derived from pressure; as the conversion between pressure and depth is linear, this difference does not affect our results or comparisons. Also note that although both of those earlier studies use potential temperature θ, we choose instead to use conservative temperature Θ, as recommended by TEOS-10 [20]. For the range of temperatures and salinities in the data we analyze, the difference $|\theta - \Theta|$ is a systematic shift that is always less than 0.05°C. Because this shift is relatively constant, our results are not sensitive to this choice. Furthermore, TEOS-10 recommends using absolute salinity S_A over practical salinity S_P. Our results do not change significantly using one versus the other (see Supplementary Materials), so we choose to use S_P to make direct comparisons to the salinity ranges used by T08 and L22.

Staircases are only found in certain vertical ranges of the water column. However, as noted by L22, the salinity values of the layers are much more consistent across different profiles than their pressure or temperature characteristics, so we focus our analyses on a specific salinity range for each ITP. While

choosing a range that is too small will potentially miss layers, running the algorithm on a liberally large range will not only take longer but may also return some clusters that do not correspond to meaningful thermohaline staircase layers. We therefore choose the salinity ranges which we know, from the earlier studies, contain the layers that we wish to identify, specifically 34.05–34.75 g/kg for ITP2 following T08 and 34.21–34.82 g/kg for ITP3 following L22.

As discussed in more detail below, the clustering algorithm does not distinguish between the different times and locations at which different profiles were taken. It follows that a dataset to be analyzed should not span larger temporal or spatial scales than the scales the staircases are known to be coherent across. T08, who analyzed much of the same data we do, found staircases that spanned the entire Canada Basin (approximately 800 km) and lasted at least 2 years. We define the longest span as the maximum distance between any two, not necessarily consecutive, profiles. We find the longest span ($\leq$ 441 km) and duration ($\leq$ 382 days) of the two ITPs we analyzed, see Table 1, are indeed smaller than the expected staircase coherence scales.

3. Methods

3.1. The HDBSCAN clustering algorithm

To identify T–S clusters as evidence for staircases within the ITP data, we use the HDBSCAN algorithm which clusters data based on the relative densities in different regions. Algorithm-identified clusters in the ITP data are expected to correspond to staircase layers, with some exceptions as detailed in Section 3.3. While Campello et al. [3] presents the algorithm in full detail, here we briefly review its general principles.

In the context of density based clustering algorithms, the term "density" refers to a measure of the relative number of data points in a certain region of parameter space. HDBSCAN estimates the density of a region based on the distances between points and a number of their nearest neighbors, creating a hierarchy of clusterings from which it chooses the most prominent. First, it calculates the "core distance" ε for each point as the minimum radius of a circle needed to encompass its m_{pts} nearest neighbors. The inverse of ε represents density; when it is small, points are close together and when it is large, points are spread out. HDBSCAN then creates a hierarchy of clusterings, starting with the largest ε and working down. For each value of ε_0, it first detects the level-set of non-noise points where $\varepsilon \leq \varepsilon_0$, then connects points together in the same cluster if they are within a distance of ε.

As the value of ε_0 decreases, a particular cluster may change by shrinking, splitting, or disappearing entirely. Having built this hierachry tree, HDBSCAN can then select clusters at the ends of branches even though different branches may terminate at very different values of ε_0. However, when the data are particularly noisy, just before crossing the ε_0 threshold where a cluster would disappear, it may split into many small, spurious clusters. To avoid including these artifacts in the final result, the algorithm ignores all clusters with fewer than m_{clSize} number of points. The recommendation of the authors of HDBSCAN and the default behavior of the "hdbscan" Python package is to set $m_{clSize} = m_{pts}$ [3, 23], giving one input parameter which controls both how the core distance is calculated and the minimum points per cluster. While there are other optional input parameters for HDBSCAN (see Supplementary Materials), the results we obtained using the default settings were satisfactory and so we did not investigate their effects.

We choose HDBSCAN over other types of clustering algorithms for several reasons. Many previous oceanographic studies used partitioning algorithms such as k-means [14, 8, 11] or Gaussian mixture models [19, 12, 36, 7]; however, partitioning algorithms require one to specify the number of clusters *a priori*, which is not known for our application. The first reason for choosing HDBSCAN is that it does not have this requirement [9, 12]. Second, HDBSCAN allows points that lie outside a cluster to be categorized as "noise." In our case, this is important because points in an interface between layers should not be assigned to any cluster. Third, unlike DBSCAN, which uses the same threshold ε_0 for all clusters throughout the domain [9, 3], HDBSCAN creates a hierarchy of clusterings with different ε_0 and can

therefore correctly identify clusters that vary significantly in both the number of points per cluster and the densities of points within the clusters [21]. Fourth, HDBSCAN can correctly identify arbitrarily shaped clusters, whereas partitioning algorithms like k-means generally find center-defined clusters, which, because points are assigned to clusters based on their distance from the cluster's center point, are only equipped to find globular, or convex, clusters [10, 9]. This is important because the shapes of clusters associated with thermohaline staircases are not necessarily globular. Lastly, HDBSCAN requires only one input parameter (m_{pts}) to be specified, reducing the number of choices to be made before each run of the algorithm. Further, we determine the value of m_{pts} systematically, as explained below.

Having chosen a clustering algorithm, we now turn to specifying the two-dimensional space within which the clustering algorithm will operate. Figure 2(a) shows data from ITP2 in Θ–S_P space, where discrete groups of points, associated with individual layers and spanning multiple profiles, are apparent; these are colored according to their eventual partitioning into clusters. Note the occurrence of occasional gaps in Θ values, seen in the salinity ranges 34.16 – 34.30 and 34.65 – 34.74 g/kg. These result from the uneven spatial coverage of the meandering drift path of the ITPs (see Figure 1) together with the tendency for the temperature to vary more horizontally within a particular layer than salinity [17]. In order to avoid HDBSCAN splitting such groups of points into multiple clusters for the same layer, for each temperature profile $\Theta(z)$, we define the local anomaly as

$$\Theta'(z) = \Theta(z) - \frac{1}{\ell}\int_{z-\ell/2}^{z+\ell/2} \Theta(z')dz' \tag{3.1}$$

where ℓ is the width of a rectangular moving average window. Presenting the ITP2 data in Θ'–S_P space rather than Θ–S_P space, as in Figure 2(c), leads to groups that are more centered around zero along the temperature axis, without notable gaps. We choose to work in this space as it will allow HDBSCAN to group points more accurately. We also confirmed the difference between using Θ or θ and S_P or S_A did not significantly affect the results. Finally, we mention that HDBSCAN is sensitive to the aspect ratio of the axes; however, because the results were found to be satisfactory, we did not investigate this dependency.

3.2. Selecting values of input parameters

It remains to choose values for the method parameters. The HDBSCAN algorithm is deterministic; that is, given the same arrangement of input data and the same value of the m_{pts} parameter, it will find the same clusters every time. The exact arrangement of data in Θ'–S_P space that we feed into the algorithm depends on three factors: (1) the set of profiles that we include, (2) the salinity range that we decide to analyze, and (3) the window width ℓ used to calculate the local anomaly of conservative temperature Θ' in Equation (3.1). We discussed our method of selecting the profiles and salinity range previously in Section 2. Here, we explain how we select values for ℓ and m_{pts}.

The results of a clustering algorithm can be judged on the basis of either external or internal validation. External validation methods involve comparing the clustering results to an external "ground truth," while internal validation methods use the data themselves to provide a measure of quality for the clustering [23]. Although we compare our results with other studies, see Section 4, these do not constitute external validations since layer labeling for individual data points, necessary to make direct comparisons, is not available from those studies. We therefore tune our selection of ℓ and m_{pts} using Density-Based Clustering Validation (DBCV) [23] as an internal validation. DBCV considers good clustering solutions to be those in which the lowest-density regions within the clusters are still denser than the highest-density regions of the surrounding noise points, basing the density estimates off the mutual reachability distance of the clusters.

To evaluate algorithm performance, we performed a parameter sweep through different values of ℓ and m_{pts}, and present the number of clusters found together with the DBCV scores in Figure 3. For the ℓ dependence, see Figure 3(a), we find a downward trend in the number of clusters as ℓ increases.

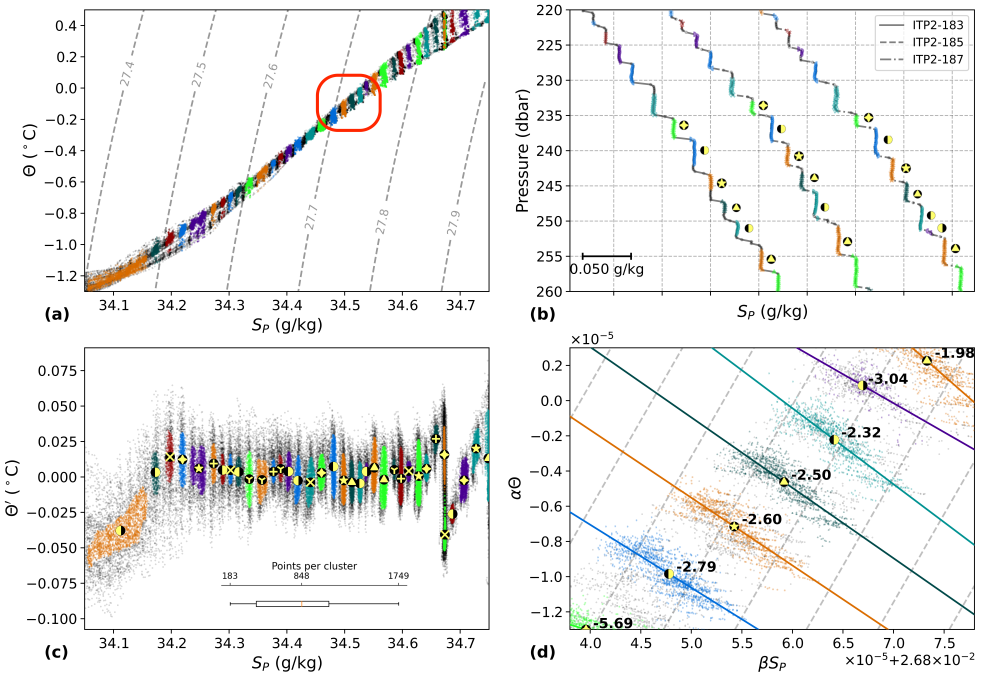

Figure 2. *Results from the clustering algorithm with $m_{pts} = 170$ and $\ell = 100$ dbar run on 53042 data points in the salinity range 34.05–34.75 g/kg from all up-going ITP2 profiles. (a) The data in Θ–S_P space with dashed lines of constant potential density anomaly (kg m^{-3}) referenced to the surface. The red box bounds the clusters marked in panels (b) and (d). (b) Profiles 183, 185, and 187 from ITP2 in a limited pressure range to show detail. Each profile is offset in S_P for clarity. (c) The spatial arrangement used as input for the algorithm where the gray points are noise and each color-marker combination indicates a cluster. The same color-marker combinations are used in each panel and the markers in panels (c) and (d) are at the cluster average for each axis. (d) A subset of the data in $\alpha\Theta$–βS_P space with the linear regression line and inverse slope (R_L) noted for each individual cluster and with dashed lines of slope $\alpha\Theta/\beta S_P = 1$.*

DBCV scores tend to be larger in the middle of the ℓ range, with the highest score occurring for $\ell = 100$ dbar. We may also note that the choice of ℓ shapes a large-scale feature of the Θ'–S_P plots. In Figure 2(c), a zig-zag pattern of increasing, rapidly decreasing, and then increasing again Θ' is seen in the range of $S_P \approx 34.63$–34.72 g/kg. This pattern is due to the presence of the AW subsurface temperature maximum in Θ profiles; it disappears when ℓ is small while becoming more exaggerated for larger ℓ (see Supplementary Materials). Based upon previous studies of staircases in the Canada Basin during this time period [44, 17], we estimated the typical layer thickness to be 5 m in height, or 5 dbar in pressure, though we found similar results for estimates of 0.5–7.5 dbar (see Supplementary Materials). The choice $\ell = 100$ dbar, where the largest DBCV score occurs, thus corresponds to approximately twenty times the typical layer thickness. This value is found to be large enough that the staircases are completely smoothed out yet small enough that the features outside the analyzed pressure range do not significantly affect the moving average.

We now turn now to m_{pts}, which under the default settings of HDBSCAN sets the minimum number of points in a cluster [3]. If the value of m_{pts} is too small, the algorithm may erroneously split a cluster that represents one layer into multiple, smaller clusters, while a too-large value of m_{pts} would lead to the incorrect grouping of multiple discrete layers into a single cluster. Note that this upper bound on a reasonable m_{pts} depends greatly on the number of data points given to the algorithm: the more data

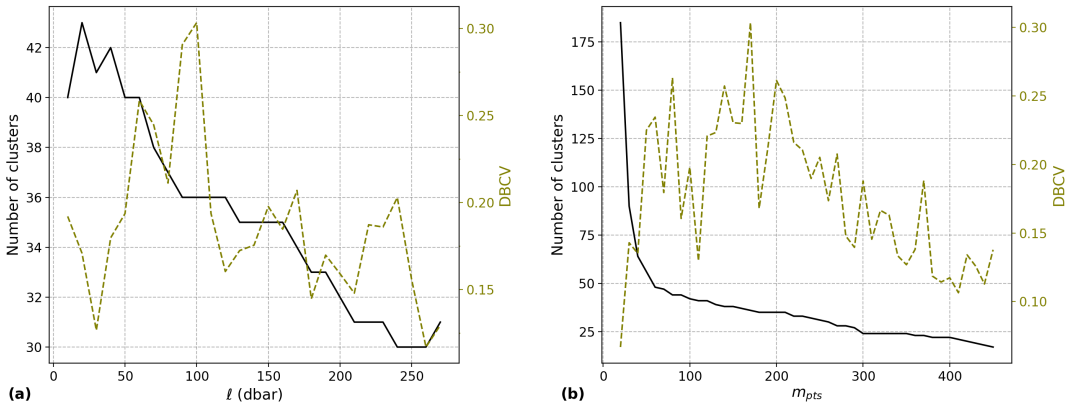

Figure 3. *A parameter sweep showing the number of clusters found (solid lines) and DBCV (dashed lines) in ITP2 as a function of (a) 27 different values of ℓ with $m_{pts} = 170$ and (b) 44 different values of m_{pts} with $\ell = 100$ dbar.*

Table 2. *The values of parameters used to run the clustering algorithm over both datasets.*

		Input Parameters				Results	
ITP	Study to Reproduce	Number of Profiles	Salinity Range (g/kg)	ℓ	m_{pts}	Number of Clusters[1]	DBCV
2	Timmermans et al. [44]	121	34.05–34.75	100 dbar	170	36 (31)	0.3034
3	Lu et al. [17]	766	34.21–34.82	100 dbar	580	43 (40)	0.3862

[1] The first number is the total number of clusters found by the algorithm. The second is the number of clusters that were neither outliers in IR_S nor R_L

points the algorithm is given, the higher the value of m_{pts} can reasonably be set. In the parameter sweep of Figure 3(b), we find the number of clusters decreases rapidly until $m_{pts} \approx 60$, then decreases at a much slower rate, while the highest DBCV scores occur for intermediate values of m_{pts}. As with ℓ, we choose the value of m_{pts} having the highest DBCV score. For ITP2, this led to our selection of $m_{pts} = 170$.

Running HDBSCAN on ITP2 using the procedure outlined above with the choices $\ell = 100$ and $m_{pts} = 170$ leads to the clusters presented in Figure 2. Following the same parameter selection process for ITP3, we obtain the values $\ell = 100$ dbar and $m_{pts} = 580$ (see Supplementary Materials). Table 2 summarizes our input parameter choices and the resulting number of clusters and DBCV values for both ITP2 and ITP3.

3.3. Evaluating the clustering algorithm results

The DBCV score gives a measure of quality for the clusters in terms of their densities of points relative to the surrounding noise. However, DBCV does not take into account the properties of the clusters that we expect from the physical situation of staircases, such as their spans in Θ and S_P or how far they are from neighboring clusters. We therefore present two metrics to help predict whether each cluster will accurately represent what we expect from layers within staircases: the lateral density ratio R_L and the normalized inter-cluster range IR.

The relative strength of horizontal variations in salinity and temperature along the ith layer is described by the lateral density ratio

$$R_L^i = \frac{\beta \Delta S_P}{\alpha \Delta \Theta}, \tag{3.2}$$

where $\beta = \rho^{-1}\partial\rho/\partial S_P$ is the haline contraction coefficient, $\alpha = -\rho^{-1}\partial\rho/\partial\Theta$ is the thermal expansion coefficient, and ΔS_P and $\Delta\Theta$ are the variations in salinity and temperature, respectively, along a particular layer [34, 2]. We estimate R_L by finding the inverse slope of the best-fit line through each cluster in $\alpha\Theta$–βS_P space (see Figure 2(d)) [44, 5]. These lines are found using Orthogonal Distance Regression, which is more suitable than ordinary least squares in our case due to the presence of variability along both the $\alpha\Theta$ and βS_P axes [49]; however, both methods yield similar results (not shown).

R_L quantifies the relative importance of S_P and Θ for the density of that layer [44, 2] and is known to be directly related to the ratio of the vertical fluxes of salinity and heat within a staircase [2]. The relative constancy of R_L values across time and space has been interpreted as reflecting the remarkable degree of lateral coherence of staircase layers [45]. Note that the lateral density ratio R_L is distinct from the density ratio, R_ρ, which is defined using the same equation (3.2) but with ΔS_P and $\Delta\Theta$ taken in the vertical direction [40]. For a cluster capturing a single complete layer, we expect the value of R_L to lie within a previously documented range [44]. Therefore, if a value of R_L lies significantly outside of this range, the cluster either reflects the erroneous grouping multiple layers into a single cluster, or else a physical merging or splitting of layers as discussed in Section 4.2.

We also define a measure of the relative spread of a variable, such as temperature or salinity, within a cluster in comparison with the differences between adjacent clusters. Ordering the clusters sequentially in density, the normalized inter-cluster range for the ith cluster is given by

$$IR_v^i = \frac{v_{max}^i - v_{min}^i}{\min(|\bar{v}^i - \bar{v}^{i-1}|, |\bar{v}^i - \bar{v}^{i+1}|)}, \tag{3.3}$$

where $i-1$ and $i+1$ denote the adjacent clusters to either side, v is the variable of interest (i.e., pressure, Θ, or S_P), v_{max}^i and v_{min}^i are the maximum and minimum values of the variable v within cluster i, and $\bar{v}^i$ denotes the mean value of v for cluster i. The numerator is the span between the maximum v_{max}^i and minimum v_{min}^i within cluster i. The denominator is the span between the mean of that cluster $\bar{v}^i$ and the mean of either the cluster above or below, whichever is smaller. For clusters at either end of the variable space, we take the denominator to be the span between the mean of the ith cluster and that of its single neighbor.

The inter-cluster range IR_v therefore quantifies the range of a given variable, v, within a cluster in comparison with the range to the nearest neighboring cluster. For a staircase, the salinity values within one layer are generally well separated from the salinity values of the neighboring layers [17]. Therefore, we expect that the clusters with large IR_{S_P} could represent a part of a single layer that was erroneously divided into multiple clusters by the algorithm, or entirely different physical features, as discussed in Section 4.3.

We define outliers in both IR_{S_P} and R_L as points with a z-score (that is, the distance from the mean divided by the standard deviation) greater than two. While this approach is not guaranteed to find all erroneous clusters, outliers in IR_{S_P} and R_L give us an indication, based on simple and measurable physical characteristics, of particular clusters which may not represent a single, full layer and which therefore require closer inspection. Although such outliers could be manually adjusted to better capture single, complete layers, we take the approach of disregarding them when calculating statistics and trends.

4. Results

Now having presented the HDBSCAN clustering algorithm, our process of selecting ℓ and m_{pts}, and metrics to identify erroneous clustering, we apply this method to data from ITP2 and ITP3.

4.1. Properties of detected layers

As a starting point, we examine the average value of pressure, Θ, or S_P for each cluster found from profiles collected by ITP3. Inspired by L22, we plot those values over time in Figure 4. We find that

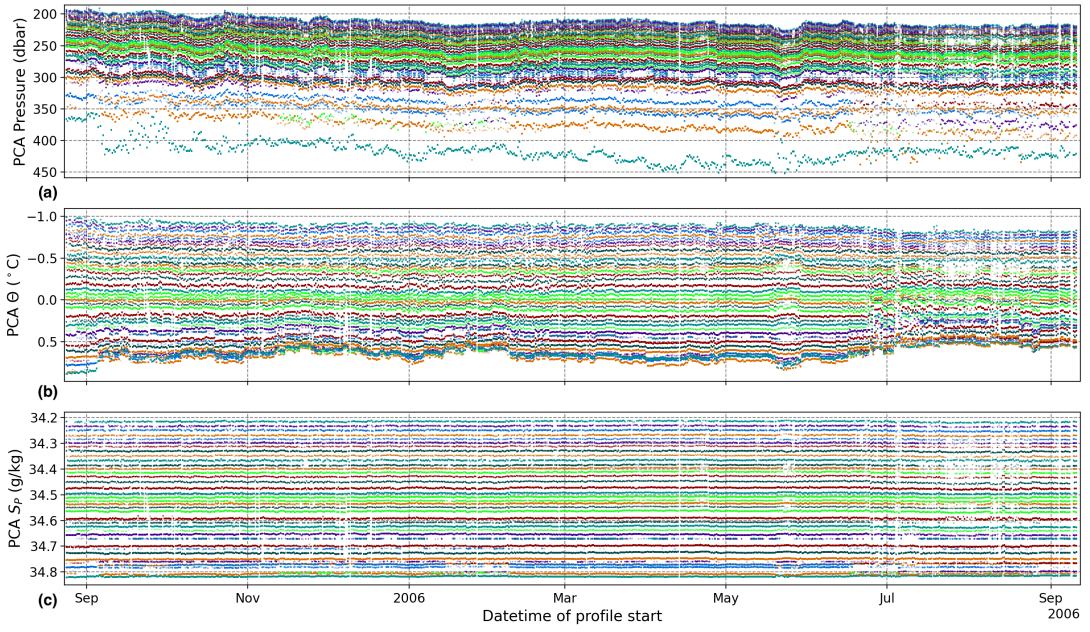

Figure 4. *The average (a) pressure, (b) Θ, and (c) S_P for the points within each cluster for each profile (profile cluster average, PCA) across time. The clustering algorithm was run with $m_{pts} = 580$ and $\ell = 100$ dbar on 678575 data points in the salinity range 34.21–34.82 g/kg from all up-going ITP3 profiles.*

Table 3. *The median normalized inter-cluster ranges and differences between average values of adjacent clusters for ITP2 and ITP3, calculated after removing outliers with z-score> 2 in the respective variable.*

	$\widehat{IR}_p$	$\widehat{IR}_\Theta$	$\widehat{IR}_{S_P}$	$\widehat{\Delta\Theta}$ (°C)	$\widehat{\Delta S_P}$ (mg/kg)
ITP2	8.394	4.087	0.707	0.048	16.5
ITP3	16.641	7.141	0.927	0.050	15.4

the clustering algorithm is capable of tracking individual layers across hundreds of profiles collected along the 2541 km-long track traced by ITP3 over 382 days. A pattern emerges, where the pressures of individual layers appear to have more variability than temperature and salinity, consistent with T08. Moreover, we find that salinity variations within a layer are smaller than the salinity differences between two neighboring layers, while the opposite is true for pressure and temperature (similar to L22; see their Figure 3). We find similar results for ITP2 (see Supplementary Materials).

More quantitatively, we find differences in salinity between clusters are approximately seven times larger than variations within a cluster. That is, we compute the standard deviation of salinity within each cluster and find that the median is 2.2 mg/kg, while the median absolute difference between the average salinity of adjacent clusters is 15.4 mg/kg. This is in agreement with L22 who found inter-layer salinity differences to be an order or magnitude larger than variations within a layer. Furthermore, the median normalized inter-cluster ranges (Equation 3.3) in Table 3 quantitatively confirm the qualitative patterns noted by T08 and L22 as $\widehat{IR}_p$, $\widehat{IR}_\Theta > 1$ and $\widehat{IR}_{S_P} < 1$ for both ITPs, where $\widehat{\cdot}$ indicates the median. Table 3 also contains the median of the differences between cluster averages of temperature, $\widehat{\Delta\Theta}$, and salinity, $\widehat{\Delta S_P}$, for both ITPs. For ITP3, these values of 0.048°C and 15.4 mg/kg match those of L22, which are 0.05°C and 17 mg/kg. They also agree with T08, who reported the the difference in temperature and salinity across interfaces to be $\delta\theta \approx 0.04$°C and $\delta S \approx 14$ mg/kg.

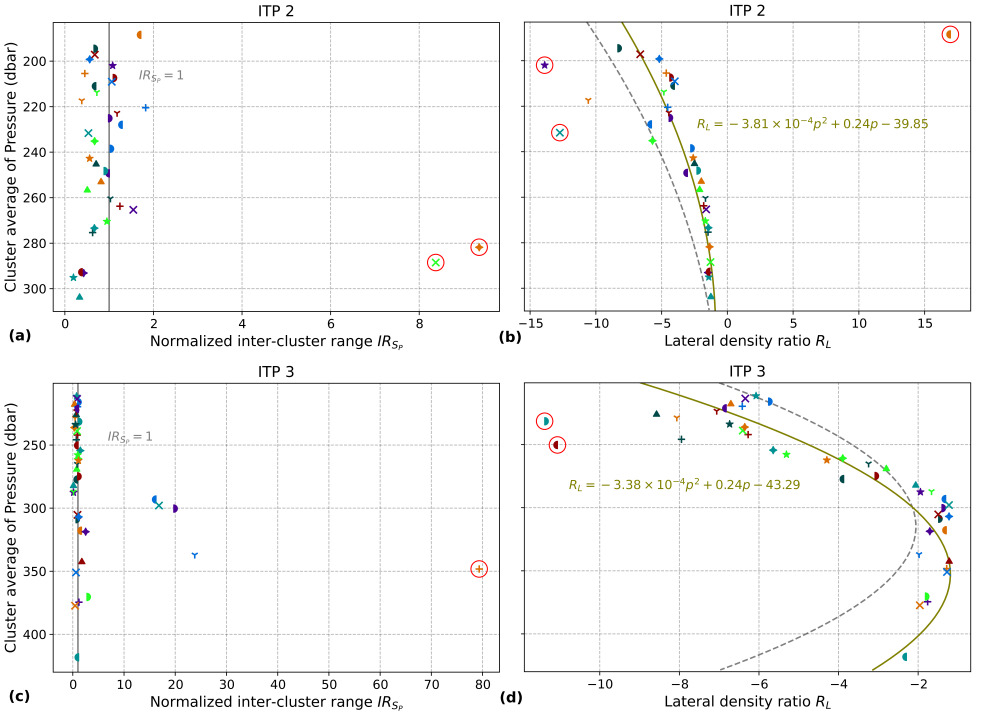

Figure 5. *The value of each cluster's normalized inter-cluster range for salinity IR_{S_P} in (a) and (c) and the lateral density ratio R_L in (b) and (d) as a function of the cluster's average pressure. The colors and markers for ITP2 in (a) and (b) are the same as the clustering shown in Figure 2 and for ITP3 in (c) and (d), they are the same as shown in Figure 4. Markers circled in red indicate outliers with a z-score greater than 2. In (b), the solid curve is a 2nd-degree polynomial fit (equation given by the annotation) for the non-outlier points from ITP2 and the dashed curve is the same for ITP3. In (d), the solid curve is a 2nd-degree polynomial fit (equation given by the annotation) for the non-outlier points from ITP3 and the dashed curve is the same for ITP2.*

4.2. Outliers and splitting / merging layers

As discussed previously in Section 3.3, outliers have been identified in the inter-cluster salinity range IR_{S_P} as well as the lateral density ratio R_L. Figure 5 shows IR_{S_P} and R_L for both ITPs with outliers indicated by red circles. We find that these outliers can either be due to erroneous clustering or indicate the presence of different physical features such as the splitting or merging of thermohaline staircase layers, which is a well-known phenomenon [27, 30, 13].

We can learn more about these features from the illustrative sets of particular salinity profiles from ITP2 presented in Figure 6. Both sets of profiles span less than a week and we narrow the displayed pressure ranges so that the individual steps are visible. This figure shows that overall, the algorithm captures the layered structure very well, marking points within interfaces as noise. Nevertheless, it is imperfect. Near layer boundaries, the algorithm sometimes includes points from an interface within a cluster, and sometimes neglects to include points within a layer. Additionally, as seen in the first profile of Figure 6(b) around 236 dbar, the algorithm can also miss layers entirely, especially when the layer is particularly thin and only present in a small number of profiles. Occasional issues such as these are to be expected with any automated detection method.

Focusing on ITP2 as an example, we find two outliers in IR_{S_P} marked by an orange 4-pointed star and a green "×" in Figure 5(a). We can track the same clusters in Figure 2(c), indicated by orange or green dots with a 4-pointed star or a "×" at the center of the cluster. They both have an average

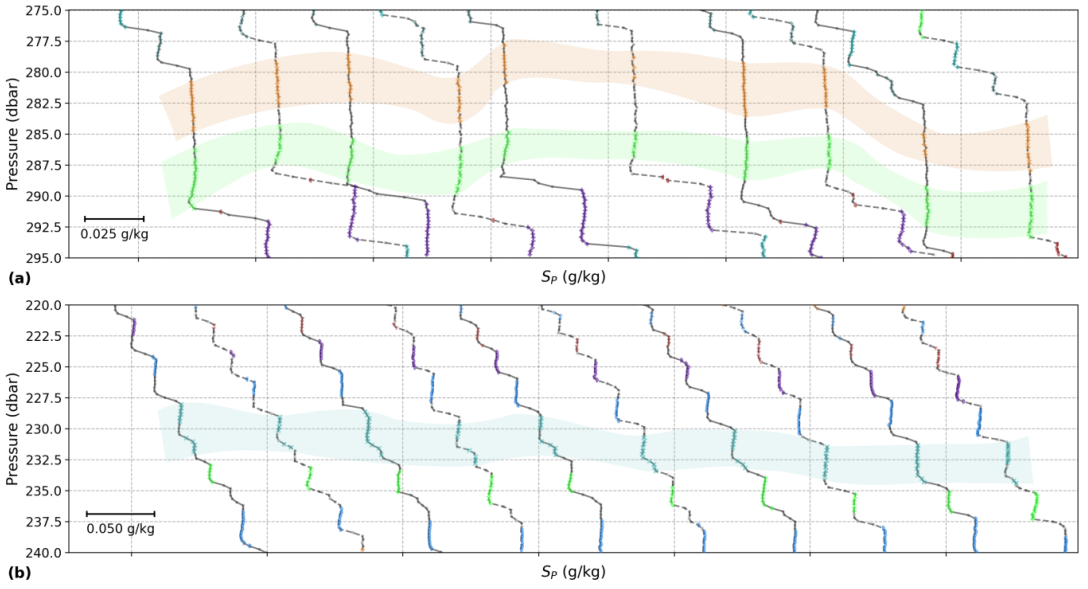

Figure 6. *Individual S_P profiles from ITP2, specifically chosen to show the examples of outlier clusters in IR_{S_P} and R_L highlighted by the bands of color. (a) Profiles 67, 69, 73, 75, 81, 83, 91, 93, 97, and 99, collected between August 31 - September 5, 2004. (b) Profiles 87, 89, 95, 97, 99, 101, 103, 105, 109, and 111, collected between September 3-7, 2004. The colors and markers are the same as the clustering shown in Figure 2. The gray dots are noise points and the black lines show the profiles. Each profile is offset in S_P for clarity .*

$S_P \approx 34.67$ g/kg but are separated in Θ'. A series of individual salinity profiles associated with these outliers over approximately six days is shown in Figure 6(a). We find that these outliers correspond to a relatively thick single layer that was erroneously split across two clusters by the algorithm. We attribute this erroneous splitting to the zig-zag pattern in Θ'–S_P space mentioned in Section 3.2 and note that it could be eliminated with a different selection of ℓ. Although we can attribute these outliers in IR_{S_P} to an artifact of the method, there are other instances where such outliers indicate the presence of physical features, as we will discuss in Section 4.3.

Next, we examine outliers in R_L, defined in Equation 3.2, for ITP2, marked by red circles in Figure 5(b). These outliers correspond to clusters that appear to have multiple layers grouped together. For example, the outlier cluster marked by an orange half-circle in Figure 5(b) can be seen in Figure 2(c) spanning $S_P = 34.054$–34.159, a much wider range than any other cluster. Similarly, in Figure 2(c), the outlier cluster marked by a purple star spans $S_P = 34.233$–34.261 and clearly encompasses what should be two distinct clusters. Some outliers in R_L are the result of erroneously clustering multiple layers together. On the other hand, the particular feature of the outlier cluster marked by a teal "×", centered around 232 dbar with $R_L = -12.7$ in Figure 5(b), indicates splitting or merging. As highlighted in Figure 6(b), it typically spans multiple stair steps, but the last few profiles it only spans a single, larger step. This illustrates that we can use outliers in R_L to identify clusters that are not single, complete layers and to find instances of potential splitting or merging.

4.3. Remnant intrusions revealed by temperature

Direct comparisons with other layer detection methods can also be used to identify interesting physical features. To demonstrate this, here we directly compare average layer characteristics computed by HDBSCAN to those reported by L22, both using data from ITP3. L22 used 758 profiles from ITP3

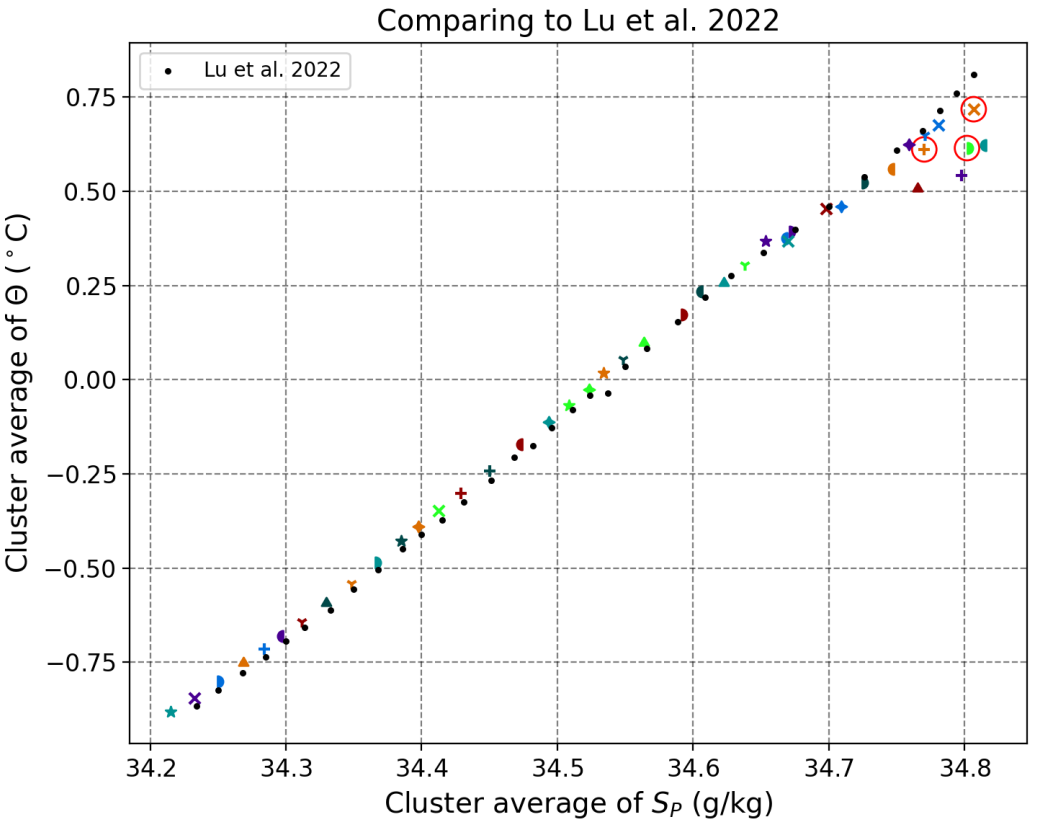

Figure 7. *The average* Θ *and* S_P *for the 34 layers found by Lu et al. [17] in black dots and for the 43 layers found in our study using data from ITP3 and the same colors and markers as in Figure 4. Clusters circled in red are outliers in either* IR_{S_P} *or* R_L*.*

while we used all 766 available up-going profiles. Based on the gaps in Figure 3 of L22, we believe that the eight missing up-going profiles are from July 2006. Figure 7 shows the average Θ and S_P for each cluster found in our study and by L22 based on the values in their Table A1 after converting θ to Θ. We initially find 43 clusters and, after eliminating outliers in IR_{S_P} and R_L as described in Section 3.3, we find 40 clusters. While L22 identified only 34 thermohaline layers, we find close agreement between those and the clusters we found for $S_P \lesssim 34.74$ g/kg. Below where this salinity occurs in the water column, we find five more clusters than L22.

The differences between these two results appears to be related to the presence of *remnant intrusions*, which display features of both staircase layers and intrusions, and are thought to represent an intermediate stage in staircase formation. Such features are known to appear near the bottom of staircases around the AW core and have been analyzed in detail by Bebieva and Timmermans [2]. They are characterized by homogeneous salinity, which leads the method of L22 to treat them as single layers. However, they have a temperature structure that is inverted (warmer above colder) compared to the typical gradient within a thermohaline staircase. The warm and cold sections are distinct enough for the clustering algorithm to split the structure into multiple clusters, each of which is homogeneous in salinity and relatively homogeneous in temperature. Figure 8 highlights an example of a remnant intrusion where the method of L22 gives results that differ from ours; the layer spanning approximately 320–340 dbar is constant

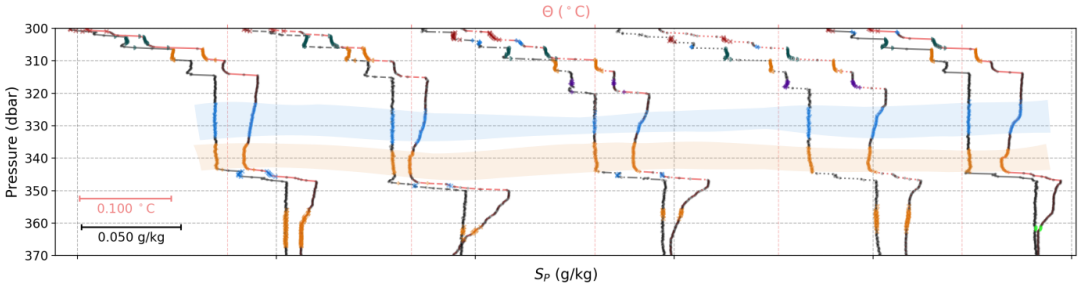

Figure 8. *Individual profiles 313, 315, 317, 319, and 321 from ITP3, collected between November 10-12, 2005, specifically chosen to show the example of a temperature inversion highlighted by the bands of color. The colors and markers of the individual points are the same as the clustering shown in Figures 4 and 7. The gray dots are noise points. The black lines on the left of each pair are the S_P profiles while the red lines on the right are for Θ. Each profile is offset in both S_P and Θ for clarity .*

in S_P, but decreases in Θ with depth and is divided into two clusters, indicated by the blue "Y" and the orange "×," using the clustering method.

Such remnant intrusions exist between the active intrusions of the AW core and the staircase layers of the LHW. Staircases may be formed from intrusions but such features have distinctly different patterns of heat and salt flux than double-diffusively driven staircases [2]. The disagreement between our results and those of L22 highlights the difficulty of detecting remnant intrusions. While neither method is designed to automatically distinguish between these and staircase layers, the method presented here offers the opportunity to identify them when evaluating outlier clusters. Moreover, although Table 3 supports the suggestion by L22 that salinity is the most appropriate variable by which to identify staircase layers, having shown that a layer identified by L22 is in fact a remnant intrusion illustrates why it remains important to consider temperature as well.

4.4. Dependence of R_L on pressure

Lastly, we revisit Figure 5(b,d) where the distribution of points suggest a dependence of R_L on pressure. This is in contrast to previous studies which have found a constant R_L for the depth range we analyze [44, 45, 2]. For ITP2 in panel (b), after removing the five outliers indicated across panels (a) and (b), we use a second-degree polynomial fit to find $R_L = -3.81 \times 10^{-4} p^2 + 0.24p - 39.85$, where p is pressure, with a coefficient of determination $R^2 = 0.67$. For ITP3 in panel (d), we remove the three outliers in panels (c) and (d) then find quite the similar dependence of $R_L = -3.38 \times 10^{-4} p^2 + 0.24p - 43.29$ with a coefficient of determination $R^2 = 0.84$. Comparing these two curves in Figure 5(b,d), we find most of the difference can be explained by a downward shift of roughly 20 dbar in the upper water column to 50 dbar in the lower water column from ITP2 to ITP3. Note that a second-degree polynomial was chosen here as a simple parameteric model to capture the apparent non-linear dependence of that R_L on pressure.

By contrast, T08 concluded there was no vertical dependence of R_L. They analyzed data from ITP1 through ITP6, which sampled the Canada Basin during the period from 2004 to 2007, and found a constant value of $R_L = -3.7 \pm 0.9$. Their Figure 6(a) shows five values of R_L for ITP2 that range from -3.5 to -3.0. While Bebieva and Timmermans [2] found that R_L changes below the depth of the temperature maximum, those authors also found in their Figure 3(b) that R_L is constant in the depth range we consider in this study. Additionally, the presence of remnant intrusions does not explain the difference in our results as the pressure dependence of R_L is evident in the upper part of the water column where they are absent. Although we find that R_L depends on pressure, our results agree with those of T08 on the magnitude of R_L, as we find the mean value for all non-outlier clusters of ITP2 to be −3.55 with a standard deviation of 2.24, and so we compare more of our results to those of T08.

We reproduce several of the figures from T08 in Figure 2. The combinations of color and markers for the clusters are the same in Figures 2, 5, and 6. In Figure 2(a), we plot data from ITP2 in Θ–S_P space, reproducing Figure 5(a) from T08. Those authors noted that points from each particular layer clustered along lines in Θ–S_P space that cross isopycnals and when we mark the clusters found by the algorithm, those layers become visually distinct. Figure 2(b) shows profile 185 in the same depth range as Figure 4 from T08, plus the up-going profiles taken by ITP2 immediately before and after. This illustrates that the clustering algorithm is indeed marking points within those particular layers as in the same cluster and points within interfaces as noise. It also shows that the clustering algorithm tracks the same layers across neighboring profiles even though the pressure at which those layers are found varies. Figure 2(c) shows the ITP2 data on the axes used by the clustering algorithm. In Figure 2(d), we plot the clusters bounded by the box in Figure 2(a) in $\alpha\Theta$–βS_P space, reproducing Figure 6(a) from T08. The dashed lines of slope 1 correspond to isopycnals as $\Delta\rho = -\alpha\Delta\Theta + \beta S_P$. Overall, the panels in Figure 2 are close visual matches for those particular figures in T08.

After examining the differences between the two in detail (see Supplementary Materials), it remains unclear why the values of R_L we found for clusters in ITP2 data differ from T08. However, we believe that the quantitative agreement in magnitude for the values of R_L and the qualitative match between the clustering results and the features in Figure 2 show that the clustering method reproduces those results from T08. Overall, these findings suggest that the clustering algorithm is indeed revealing a dependence of R_L on pressure in the data we analyzed from ITP2 and ITP3. Since R_L is directly related to the ratio of the vertical derivatives of the vertical fluxes of salinity and heat within a staircase [2], this could indicate a pressure dependence of that ratio.

5. Discussion

In this paper, we have presented a method based on the HDBSCAN clustering algorithm to both detect and connect well-mixed layers in thermohaline staircases across Arctic Ocean hydrographic data. HDBSCAN has previously been successfully applied to sets with millions of data points [16]. As the comparison with results from previous studies was favorable, this suggests that this method would produce trustworthy results when applied to datasets with larger numbers of points. This study contributes to a growing set of examples of clustering algorithms being used in oceanography [e.g., 14, 8, 19, 18, 12, 11, 36, 7, 41]. The continued and extended use of clustering algorithms in oceanography and related fields is an important development, since discovering and detecting features in all manner of datasets becomes more challenging as they grow ever larger.

Special attention was given herein to the identification of outliers using parameters output by the method itself. We found that clusters which are outliers in the lateral density ratio R_L often indicate multiple layers that are erroneously clustered together, but can also highlight potential instances of layer splitting or merging. By introducing the normalized inter-cluster range IR_v, we quantitatively showed that the pressure and temperature values vary more within a layer than the difference between the values of neighboring layers, while the opposite is true for salinity. Because we know that the practical salinity S_P values in a particular layer are well separated from those of neighboring layers, we identified clusters with notably large values of IR_{S_P} as likely to be either only part of a layer that was erroneously split by the algorithm or a remnant intrusion. An apparently new result from this study is the pressure dependence of the lateral density ratio R_L, seen in both ITP2 and ITP3. The reasons for this dependence are unclear and are worthy of further study. Following the model presented by Bebieva and Timmermans [2], the ratio of vertical fluxes of heat and salt could be recalculated using this more complex vertical dependence of R_L. This could then be compared to simulations [50] and parameterizations [35, 39] of the flux ratio in other models. However, in order to verify these with observations, vertical resolution fine enough to resolve the interfaces between layers, that is, finer than provided by ITPs, would be needed.

The method we presented here has certain advantages over other staircase detection techniques. For example, all of the other methods referred to herein [44, 40, 48, 17] require setting one or multiple thresholds on gradients in temperature, salinity, or density which are used to identify sections of profiles

where layers may be present. However, choosing reasonable values for these thresholds requires precise prior knowledge of the staircase properties, which may not be available before identifying staircases in that particular region and time period. The method presented here requires the selection of a salinity range in which to search and an estimate of the typical layer thickness which can be determined from a brief look at a dataset or from previous studies. In addition, while the other techniques require resolution high enough to resolve small-scale vertical gradients, the method presented here—which does not distinguish between individual profiles—only requires that a sufficient number of data points be available in order to detect clusters. Therefore, this technique could potentially find staircases in datasets that have too low a resolution to resolve the steps in any particular profile. While, in this study, we use all data points available after filtering, we found that subsampling profiles to every second, third, or fourth point yielded similar results (not shown). Finally, the method automatically connects layers across profiles. While L22 used an automated connection method, it still required subsequent adjustments to the layers to be made manually. Consequently the method presented here could be readily applied to datasets with larger numbers of points and used to examine the large-scale, lateral properties of layers in thermohaline staircases.

The clustering algorithm has several limitations. It cannot be used to examine sets of profiles spanning temporal or spatial scales larger than those on which stairs are known to be coherent. This method considers all profiles simultaneously, and it is not applicable to identifying stair steps in datasets of independent individual profiles. While this method could be applied on a profile-by-profile basis, each profile would require a separate selection of m_{pts} which itself becomes highly sensitive with a small number of points to cluster. Moreover, as the clustering algorithm does not consider profiles individually, it may miss layers which are only present in a small number of profiles, as may occur especially for layers that split or merge. Finally, although the clustering method captures the overall structure of the staircase layers well, it sometimes miscategorizes points, especially near the boundaries between layers and interfaces.

The method presented here could be used in conjunction with other staircase detection methods. For example, if a different detection method were used to identify which data points in a collection of profiles are in layers, the clustering algorithm could be run on just the layer points to automatically connect the layers across profiles. Additionally, the clustering algorithm could be used on a large collection of datasets to identify which subsets contain staircases; then a more specifically tuned staircase detection method could be used on just that subset, reducing the amount of time-consuming analysis.

Because the method can be scaled to datasets with a larger number of points, a natural extension would be to apply it to more ITP profiles. Furthermore, although we have focused on identifying upper-ocean Arctic thermohaline staircases, it could also be useful in other oceanic regimes. Staircases with steps on the order of 50 m thick have been observed in the Arctic between depths of 2000–3000 m [43], much deeper than ITPs measure, while the Argo network of autonomous profiling floats has captured staircases in regions all over the world [47]. Since this method does not assume a consistent vertical resolution across the profiles, it could be run on a mix of data from different types of instruments, assuming they operated within the same region and time period. This method could also be adjusted to identify other structures that appear in Θ–S space such as different types of layers or water masses, or even structures that can appear in different spaces such as Θ–O_2 [36]. On the technical side, another topic of future study would be to adapt this method to automatically distinguish between well-mixed layers and intrusions. However, when using this clustering algorithm to specifically search for staircase layers, we recommend avoiding the bottom of the thermocline around the AW core where remnant intrusions are known to appear [2]. Finally, there may be methods other than the DBCV validation process used herein that may be better able to guide the choice of parameters, potentially improving the detection fidelity.

Acknowledgments. This research was supported in part by the National Science Foundation under Grant No. NSF PHY-1748958. We acknowledge fruitful discussions with Maike Sonnewald and Carine van der Boog. E.R. is grateful to the researchers, staff and students of the Centre for Earth Observation Science for support received during preparation of this manuscript.

Funding Statement. M.G.S. and N.G. were supported by the Natural Sciences and Engineering Research Council of Canada (NSERC) [funding reference numbers RGPIN-2015-03684 and RGPIN-2022-04560]. J.M.L. was supported by grant number 2049521 from the Physical Oceanography program of the United States National Science Foundation. ER was supported by the National Sciences and Engineering Research Council of Canada (NSERC) PDF award and the NSERC Canada-150 Chair (Award G00321321).

Competing Interests. The authors declare none.

Data Availability Statement. Replication code can be found on Zenodo: https://zenodo.org/record/8173386. The Ice-Tethered Profiler data were collected and made available by the Ice-Tethered Profiler Program (Toole et al. [45], Krishfield et al. [15]) based at the Woods Hole Oceanographic Institution (https://www2.whoi.edu/site/itp/).

Ethical Standards. The research meets all ethical guidelines, including adherence to the legal requirements of the study country.

Author Contributions. Conceptualization: M.G.S., N.G., E.R., J.M.L.; Data Curation: M.G.S.; Formal Analysis: M.G.S.; Funding Acquisition: N.G.; Investigation: M.G.S.; Methodology: M.G.S.; Software: M.G.S.; Supervision: N.G., E.R., J.M.L.; Validation: M.G.S., N.G., E.R., J.M.L.; Visualization: M.G.S.; Writing – Original Draft: M.G.S.; Writing – Review & Editing: M.G.S., N.G., E.R., J.M.L.; All authors approved the final submitted draft.

References

[1] André, Q., Barker, A. J., & Mathis, S. (2017). Layered semi-convection and tides in giant planet interiors. *Astronomy & Astrophysics*, *605*, A117, https://doi.org/10.1051/0004-6361/201730765.

[2] Bebieva, Y. & Timmermans, M. L. (2019). Double-Diffusive Layering in the Canada Basin: An Explanation of Along-Layer Temperature and Salinity Gradients. *Journal of Geophysical Research: Oceans*, *124*(1), 723–735, https://doi.org/10.1029/2018JC014368.

[3] Campello, R. J. G. B., Moulavi, D., & Sander, J. (2013). Density-Based Clustering Based on Hierarchical Density Estimates. *Lecture Notes in Computer Science*, *7819*, 160–172, https://doi.org/10.1007/978-3-642-37456-2_14.

[4] Carmack, E. C. (2007). The alpha/beta ocean distinction: A perspective on freshwater fluxes, convection, nutrients and productivity in high-latitude seas. *Deep-Sea Research Part II: Topical Studies in Oceanography*, *54*(23-26), 2578–2598, https://doi.org/10.1016/j.dsr2.2007.08.018.

[5] Chen, L. G. (1995). Mixed Layer Density Ratio from the Levitus Data. *Journal of Physical Oceanography*, *25*(4), 691–701, https://doi.org/10.1175/1520-0485(1995)025<0691:MLDRFT>2.0.CO;2.

[6] Comiso, J. C., Parkinson, C. L., Gersten, R., & Stock, L. (2008). Accelerated decline in the Arctic sea ice cover. *Geophysical Research Letters*, *35*(1), 1–6, https://doi.org/10.1029/2007GL031972.

[7] Desbruyères, D., Chafik, L., & Maze, G. (2021). A shift in the ocean circulation has warmed the subpolar North Atlantic Ocean since 2016. *Communications Earth & Environment*, *2*(1), https://doi.org/10.1038/s43247-021-00120-y.

[8] Espejo, A., Camus, P., Losada, I. J., & Méndez, F. J. (2014). Spectral Ocean Wave Climate Variability Based on Atmospheric Circulation Patterns. *Journal of Physical Oceanography*, *44*(8), 2139–2152, https://doi.org/10.1175/JPO-D-13-0276.1.

[9] Ester, M., Kriegel, H.-P., Sander, J., & Xu, X. (1996). A Density-Based Algorithm for Discovering Clusters in Large Spatial Databases with Noise. In *Proceedings of the Second International Conference on Knowledge Discovery and Data Mining* (pp. 226–231). Elsevier.

[10] Hinneburg, A. & Keim, D. A. (2003). A General Approach to Clustering in Large Databases with Noise. *Knowledge and Information Systems*, *5*(4), 387–415, https://doi.org/10.1007/s10115-003-0086-9.

[11] Houghton, I. A. & Wilson, J. D. (2020). El Niño Detection Via Unsupervised Clustering of Argo Temperature Profiles. *Journal of Geophysical Research: Oceans*, *125*(9), 1–12, https://doi.org/10.1029/2019JC015947.

[12] Jones, D. C., Holt, H. J., Meijers, A. J., & Shuckburgh, E. (2019). Unsupervised Clustering of Southern Ocean Argo Float Temperature Profiles. *Journal of Geophysical Research: Oceans*, *124*(1), 390–402, https://doi.org/10.1029/2018JC014629.

[13] Kimura, S., Nicholls, K. W., & Venables, E. (2015). Estimation of Ice Shelf Melt Rate in the Presence of a Thermohaline Staircase. *Journal of Physical Oceanography*, *45*(1), 133–148, https://doi.org/10.1175/JPO-D-14-0106.1.

[14] Koszalka, I. M. & LaCasce, J. H. (2010). Lagrangian analysis by clustering. *Ocean Dynamics*, *60*(4), 957–972, https://doi.org/10.1007/s10236-010-0306-2.

[15] Krishfield, R., Toole, J., & Timmermans, M. (2008). ITP Data Processing Procedures. *Woods Hole Oceanographic Institution*, (March), 1–24.

[16] Logan, C. H. A. & Fotopoulou, S. (2020). Unsupervised star, galaxy, QSO classification. *Astronomy & Astrophysics*, *633*, A154, https://doi.org/10.1051/0004-6361/201936648.

[17] Lu, Y.-Z., Guo, S.-X., Zhou, S.-Q., Song, X.-L., & Huang, P.-Q. (2022). Identification of Thermohaline Sheet and Its Spatial Structure in the Canada Basin. *Journal of Physical Oceanography*, *52*(11), 2773–2787, https://doi.org/10.1175/JPO-D-22-0012.1.

[18] Ma, C., Li, S., Yang, Y., Yang, J., & Chen, G. (2019). Extraction of Revolving Channels of Drifters around Mesoscale Eddy Centers Based on Spatiotemporal Trajectory Clustering. *Journal of Atmospheric and Oceanic Technology*, *36*(9), 1903–1916, https://doi.org/10.1175/JTECH-D-19-0007.1.

[19] Maze, G., et al. (2017). Coherent heat patterns revealed by unsupervised classification of Argo temperature profiles in the North Atlantic Ocean. *Progress in Oceanography*, *151*, 275–292, https://doi.org/10.1016/j.pocean.2016.12.008.

[20] McDougall, T. J. & Barker, P. M. (2011). Getting started with TEOS-10 and the Gibbs Seawater (GSW) Oceanographic Toolbox. 3.06.12 edition www.TEOS-10.org.

[21] McInnes, L., Healy, J., & Astels, S. (2017). hdbscan: Hierarchical density based clustering. *The Journal of Open Source Software*, *2*(11), 205, https://doi.org/10.21105/joss.00205.

[22] Ménesguen, C., Lique, C., & Caspar-Cohen, Z. (2022). Density Staircases Are Disappearing in the Canada Basin of the Arctic Ocean. *Journal of Geophysical Research: Oceans*, *127*(11), https://doi.org/10.1029/2022JC018877.

[23] Moulavi, D., Jaskowiak, P. A., Campello, R. J. G. B., Zimek, A., & Sander, J. (2014). Density-Based Clustering Validation. In *Proceedings of the 2014 SIAM International Conference on Data Mining*, volume 2 (pp. 839–847). Philadelphia, PA: Society for Industrial and Applied Mathematics https://epubs.siam.org/doi/10.1137/1.9781611973440.96.

[24] Neal, V. T. & Neshyba, S. (1973). Microstructure Anomalies in the Arctic Ocean. *Journal of Geophysical Research*, *78*(15), 2695–2701, https://doi.org/10.1029/JC078i015p02695.

[25] Neal, V. T., Neshyba, S., & Denner, W. (1969). Thermal Stratification in the Arctic Ocean. *Science*, *166*(3903), 373–374, https://doi.org/10.1126/science.166.3903.373.

[26] Neshyba, S., Neal, V. T., & Denner, W. (1971). Temperature and Conductivity Measurements under Ice Island T-3. *Journal of Geophysical Research*, *76*(33), 8107–8120, https://doi.org/10.1029/JC076i033p08107.

[27] Neshyba, S., Neal, V. T., & Denner, W. W. (1972). Spectra of Internal Waves: In-Situ Measurements in a Multiple-Layered Structure. *Journal of Physical Oceanography*, *2*(1), 91–95, https://doi.org/10.1175/1520-0485(1972)002<0091:SOIWSM>2.0.CO;2.

[28] Newman, F. C. (1976). Temperature Steps in Lake Kivu: A Bottom Heated Saline Lake. *Journal of Physical Oceanography*, *6*(2), 157–163, https://doi.org/10.1175/1520-0485(1976)006<0157:TSILKA>2.0.CO2.

[29] Padman, L. & Dillon, T. M. (1987). Vertical Heat Fluxes Through the Beaufort Sea Thermohaline Staircase. *Journal of Geophysical Research*, *92*(C10), 10799, https://doi.org/10.1029/JC092iC10p10799.

[30] Padman, L. & Dillon, T. M. (1988). On the Horizontal Extent of the Canada Basin Thermohaline Steps. *Journal of Physical Oceanography*, *18*(10), 1458–1462, https://doi.org/10.1175/1520-0485(1988)018<1458:OTHEOT>2.0.CO;2.

[31] Padman, L. & Dillon, T. M. (1989). Thermal microstructure and internal waves in the Canada Basin diffusive staircase. *Deep Sea Research Part A, Oceanographic Research Papers*, *36*(4), 531–542, https://doi.org/10.1016/0198-0149(89)90004-6.

[32] Peralta-Ferriz, C. & Woodgate, R. A. (2015). Seasonal and interannual variability of pan-Arctic surface mixed layer properties from 1979 to 2012 from hydrographic data, and the dominance of stratification for multiyear mixed layer depth shoaling. *Progress in Oceanography*, *134*, 19–53, https://doi.org/10.1016/j.pocean.2014.12.005.

[33] Pontin, C. M., Barker, A. J., Hollerbach, R., André, Q., & Mathis, S. (2021). Wave propagation in semiconvective regions of giant planets. *Monthly Notices of the Royal Astronomical Society*, *493*(4), 5788–5806, https://doi.org/10.1093/mnras/staa664.

[34] Radko, T. (2013). Double-Diffusive Convection. Cambridge University Press https://doi.org/10.1017/CBO9781139034173.

[35] Radko, T., Bulters, A., Flanagan, J. D., & Campin, J. M. (2014). Double-diffusive recipes. Part I: Large-scale dynamics of thermohaline staircases. *Journal of Physical Oceanography*, *44*(5), 1269–1284, https://doi.org/10.1175/JPO-D-13-0155.1.

[36] Rosso, I., Mazloff, M. R., Talley, L. D., Purkey, S. G., Freeman, N. M., & Maze, G. (2020). Water Mass and Biogeochemical Variability in the Kerguelen Sector of the Southern Ocean: A Machine Learning Approach for a Mixing Hot Spot. *Journal of Geophysical Research: Oceans*, *125*(3), 1–23, https://doi.org/10.1029/2019JC015877.

[37] Schmitt, R., Perkins, H., Boyd, J., & Stalcup, M. (1987). C-SALT: an investigation of the thermohaline staircase in the western tropical North Atlantic. *Deep Sea Research Part A. Oceanographic Research Papers*, *34*(10), 1655–1665, https://doi.org/10.1016/0198-0149(87)90014-8.

[38] Shaw, W. J. & Stanton, T. P. (2014). Vertical diffusivity of the Western Arctic Ocean halocline. *Journal of Geophysical Research: Oceans*, *119*(8), 5017–5038, https://doi.org/10.1002/2013JC009598.

[39] Shibley, N. C. & Timmermans, M.-L. (2019). The Formation of Double-Diffusive Layers in a Weakly Turbulent Environment. *Journal of Geophysical Research: Oceans*, https://doi.org/10.1029/2018JC014625.

[40] Shibley, N. C., Timmermans, M.-L., Carpenter, J. R., & Toole, J. M. (2017). Spatial variability of the Arctic Ocean's double-diffusive staircase. *Journal of Geophysical Research: Oceans*, *122*(2), 980–994, https://doi.org/10.1002/2016JC012419.

[41] Sonnewald, M., Lguensat, R., Jones, D. C., Dueben, P. D., Brajard, J., & Balaji, V. (2021). Bridging observations, theory and numerical simulation of the ocean using machine learning. *Environmental Research Letters*, *16*(7), 073008, https://doi.org/10.1088/1748-9326/ac0eb0.

[42] Stewart, K. D. & Haine, T. W. (2016). Thermobaricity in the transition zones between alpha and beta oceans. *Journal of Physical Oceanography*, *46*(6), 1805–1821, https://doi.org/10.1175/JPO-D-16-0017.1.

[43] Timmermans, M.-l., Garrett, C., & Carmack, E. (2003). The thermohaline structure and evolution of the deep waters in the Canada Basin, Arctic Ocean. *Deep Sea Research Part I: Oceanographic Research Papers*, *50*, 1305–1321, https://doi.org/10.1016/S0967-0637(03)00125-0.

[44] Timmermans, M.-L., Toole, J., Krishfield, R., & Winsor, P. (2008). Ice-Tethered Profiler observations of the double-diffusive staircase in the Canada Basin thermocline. *Journal of Geophysical Research*, *113*, 1–10, https://doi.org/10.1029/2008jc004829.

[45] Toole, J. M., Krishfield, R. A., Timmermans, M. L., & Proshutinsky, A. (2011). The Ice-Tethered profiler: Argo of the Arctic. *Oceanography*, *24*(3), 126–135, https://doi.org/10.5670/oceanog.2011.64.

[46] Turner, J. S. (2010). The Melting of Ice in the Arctic Ocean: The Influence of Double-Diffusive Transport of Heat from Below. *Journal of Physical Oceanography*, *40*(1), 249–256, https://doi.org/10.1175/2009JPO4279.1.

[47] van der Boog, C. G., Dijkstra, H. A., Pietrzak, J. D., & Katsman, C. A. (2021a). Double-diffusive mixing makes a small contribution to the global ocean circulation. *Communications Earth & Environment*, *2*(1), 46, https://doi.org/10.1038/s43247-021-00113-x.

[48] van der Boog, C. G., Otto Koetsier, J., Dijkstra, H. A., Pietrzak, J. D., & Katsman, C. A. (2021b). Global dataset of thermohaline staircases obtained from Argo floats and Ice-Tethered Profilers. *Earth System Science Data*, *13*(1), 43–61, https://doi.org/10.5194/essd-13-43-2021.

[49] Winton, M. (2011). Do Climate Models Underestimate the Sensitivity of Northern Hemisphere Sea Ice Cover? *Journal of Climate*, *24*(15), 3924–3934, https://doi.org/10.1175/2011JCLI4146.1.

[50] Yang, Y., Verzicco, R., Lohse, D., & Caulfield, C. (2022). Layering and vertical transport in sheared double-diffusive convection in the diffusive regime. *Journal of Fluid Mechanics*, *933*, A30, https://doi.org/10.1017/jfm.2021.1091.

[51] Yu, L. S., Bosse, A., Fer, I., Orvik, K. A., Bruvik, E. M., Hessevik, I., & Kvalsund, K. (2017). The Lofoten Basin eddy: Three years of evolution as observed by Seagliders. *Journal of Geophysical Research: Oceans*, *122*(8), 6814–6834, https://doi.org/10.1002/2017JC012982.

METHODS PAPER

Supplementary Materials for: Unsupervised clustering identifies thermohaline staircases in the Canada Basin of the Arctic Ocean

Mikhail G. Schee[1], Erica Rosenblum[1,2], Jonathan M. Lilly[3] and Nicolas Grisouard[1]

[1]Department of Physics, University of Toronto, Toronto, M5S 1A7, Ontario, Canada, E-mail: mikhail.schee@mail.utoronto.ca.
[2]Centre for Earth Observation Science, University of Manitoba, Winnipeg, R3T 2M6, Manitoba, Canada.
E-mail: erica.j.rosenblum@gmail.com.
[3]Planetary Science Institute, Tucson, 85719, Arizona, USA. E-mail: jmlilly@psi.edu.

Keywords: Arctic Ocean, clustering algorithm, machine learning, thermohaline staircases, ice-tethered profilers

S. Supplementary materials

S.1. Practical salinity S_P vs. absolute salinity S_A

TEOS-10 recommends storing values of practical salinity S_P in databases in order to maintain continuity with older records and also because S_P is practically a measured quantity [20]. In contrast, absolute salinity S_A is a calculated variable defined as "the mass fraction of dissolved non-H_2O material in a seawater sample at its temperature and pressure," and is recommended for use in publications [**?**]. For this study, we ultimately chose to work with S_P because the two studies to which we make direct comparisons, T08 and L22, used S_P. Specifically, when we define the ranges of S_P to filter to before running the clustering algorithm, we were able to directly take the values of S_P from T08 and L22 without having to first convert to S_A.

To investigate the difference between using S_P vs. S_A on our results, we recreated Figure 2, but replacing S_P with S_A on all the axes, as shown in Figure S.1. We still filtered the ITP2 data to be in the practical salinity range S_P 34.05–34.75 g/kg to make sure we used the same data points. However, then we plotted those data points in Θ'–S_A space in panel (c) to run the clustering algorithm using the same $m_{pts} = 170$. This resulted in 38 clusters (as opposed to 36) with a DBCV score of 0.2177 (as opposed to 0.3034). In panel (d), the values of R_L displayed made minor changes of (from left to right): +0.39, -0.04, -0.03, -0.03, -0.01, +0.14, and +0.07.

We also reproduced Figure 5(a,b) in Figure S.2 using the clustering shown in Figure S.1. The two outliers in IR_{S_A} in Figure S.2(a) do not correspond to outliers in Figure 5(a) because these have very high IR_{S_A}, over 20, which skews the mean as used when calculating the z-score. The dark green star and the red triangle in Figure S.2(a) correspond to the two outliers in Figure 5(a) where they are marked by an orange 4-pointed star and a green "×". These pairs of points have very similar values of IR_{S_A} and IR_{S_P}, respectively.

In Figure S.2(b), we see that there are two outliers in R_L circled, both of which correspond to outliers found when using S_P. The purple star in Figure S.2(b) corresponds to the orange left half circle in Figure 5(b), while the dark green "Y" in Figure S.2(b) corresponds to the teal "×" in Figure 5(b). A notable difference is that the purple star outlier in Figure 5(b) (which spans $S_P = 34.233$–34.261 in Figure 2(c) encompassing what should be two distinct clusters) is no longer present in Figure S.2(b). Comparing Figures 2(c) and S.1(c), we see that it is now replaced by two clusters, the dark green left half circle and the red right half circle, neither of which are outliers in R_L.

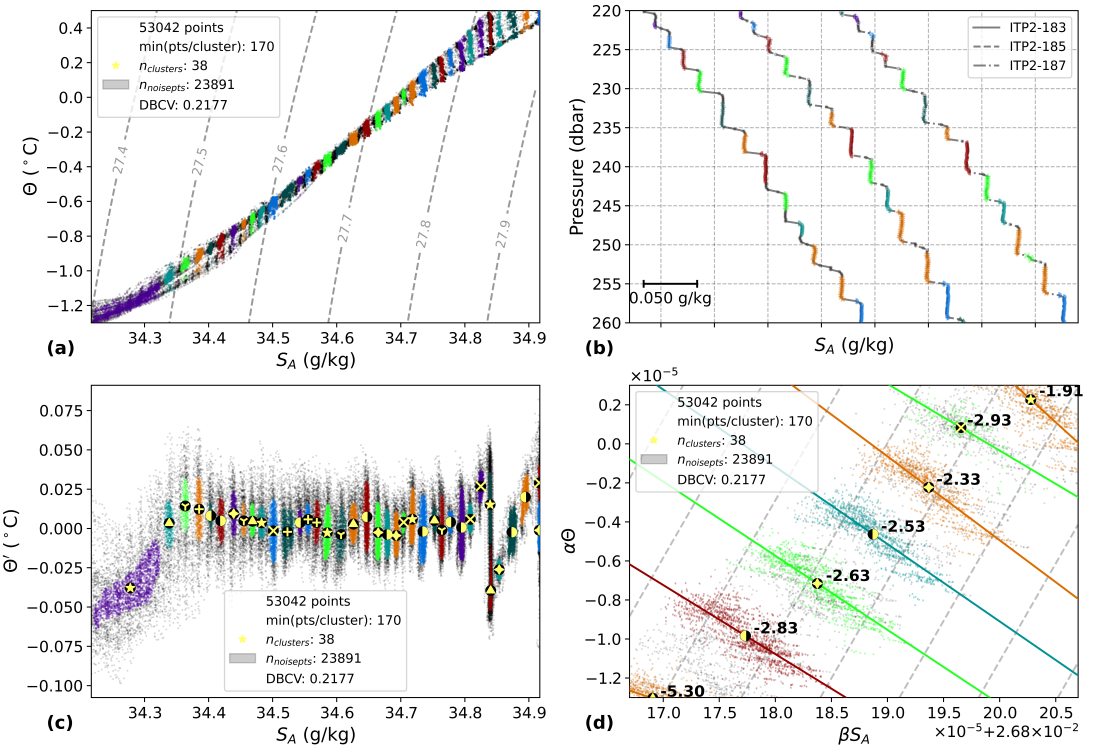

Figure S.1. *Results from the clustering algorithm with $m_{pts} = 170$ and $\ell = 100$ dbar run on 53042 data points in the S_P range 34.05–34.75 g/kg from all up-going ITP2 profiles. This is the same as Figure 2, but the clustering algorithm was run on absolute salinity S_A instead of practical salinity S_P. (a) The data in Θ–S_A space with dashed lines of constant potential density anomaly (kg m^{-3}) referenced to the surface. (b) Profiles 183, 185, and 187 from ITP2 in a limited pressure range to show detail. Each profile is offset in S_A for clarity. (c) The spatial arrangement used as input for the algorithm where the gray points are noise and each color-marker combination indicates a cluster. The same color-marker combinations are used in each panel and the markers in panels (c) and (d) are at the cluster average for each axis. (d) A subset of the data in $\alpha\Theta$–βS_A space with the linear regression line and inverse slope (R_L) noted for each individual cluster and with dashed lines of slope $\alpha\Theta/\beta S_A = 1$.*

We also see that the 2nd-degree polynomial fit in Figure S.2(b) is similar to that in Figure 5(b). We conclude that the difference between using S_A vs. S_P does not significantly affect our results.

S.2. Varying the value of ℓ

We define the local anomaly of a temperature profile Θ' as the original profile minus a version of that profile smoothed with a moving average. Subtracting a smoothed profile from the original profile in this way gives temperature differences that are centered around zero and leads to more continuous clusters (compare Figures 2(a) and 2(c)), allowing HDBSCAN to group these points more accurately.

When calculating Θ' with Equation 3.1, we use a moving average with window size ℓ, so the resulting profile has dead regions $\ell/2$ in size with no data at the top and bottom. Therefore, ℓ cannot be larger than twice the distance available in the profile, either above or below the pressure range to be analyzed, whichever is smaller. As ℓ increases, the moving average profile gets flatter, meaning Θ' becomes closer to the original profile, just shifted in temperature space. Choosing a very small ℓ will give a moving average temperature profile that will closely match the original temperature profile, meaning that the Θ'

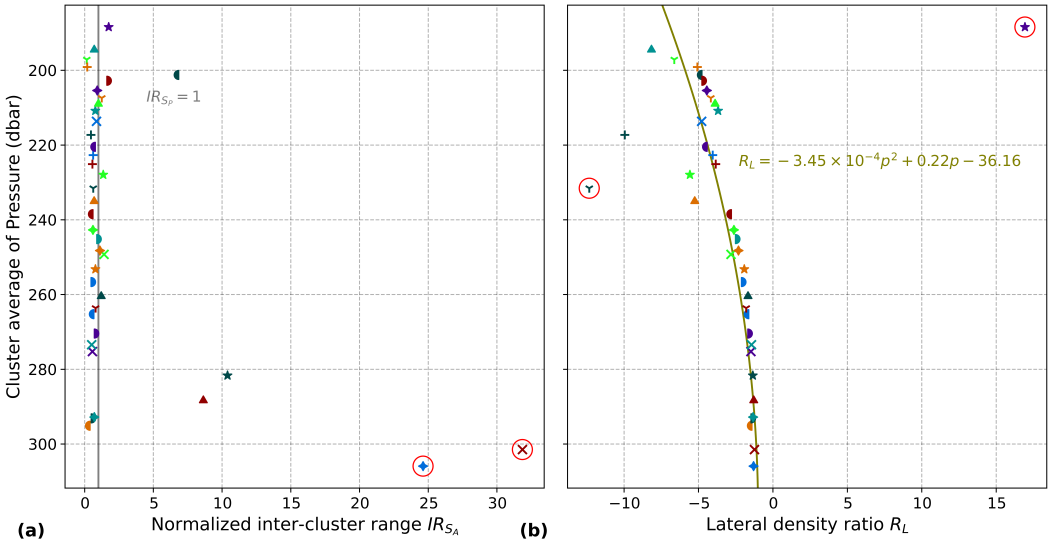

Figure S.2. *The value of each cluster's normalized inter-cluster range for salinity IR_{S_A} in (a) and the lateral density ratio R_L in (b) as a function of the cluster's average pressure for ITP2. This is the same as Figure 5(a,b), but the clustering algorithm was run on absolute salinity S_A instead of practical salinity S_P. The colors and markers are the same as the clustering shown in Figure S.1. Markers circled in red indicate outliers with a z-score greater than* 2*.*

profile will be very close to zero. This eliminates any effect temperature might have on the clustering results.

In Figure S.3, we show 4 pairs of profiles, restricted to the 200-400 dbar pressure range to show detail. All profiles are number 185 from ITP2, the example profile featured in Figure 2(b). Each panel shows both the original profile and the moving average profile with the values of ℓ: 10, 50, 100, and 150 dbar. The original and moving average profiles are slightly offset for clarity. When $\ell = 10$ dbar, the moving average profile still clearly contains some of the larger stair steps. When $\ell = 150$ dbar, almost all of the features in the original profile are gone.

We noted a feature in 2(c) where the cluster average Θ' increases starting at $S_P \approx 34.63$ g/kg until it jumps sharply to negative Θ' values around $S_P \approx 34.67$ g/kg, then increases again until $S_P \approx 34.72$ g/kg. This zig-zag pattern is due to the choice of ℓ and the presence of the AW subsurface temperature maximum in Θ profiles. In Figure S.4, we show the ITP2 data used in the study in Θ'–S_P space for the same 4 values of ℓ as in Figure S.3. This clearly illustrates that the zig-zag pattern is not present for low ℓ and becomes more pronounced as ℓ increases.

For each panel in Figure S.4, we ran a parameter sweep across m_{pts} similar to that shown in Figure 3(b), selecting the value of m_{pts} which gave the highest DBCV, as shown in the legends. If we always choose ℓ to be approximately twenty times the typical layer thickness, then the panels in Figure S.4 represent clusterings for thickness estimates of 0.5 dbar, 2.5 dbar, 5 dbar, and 7.5 dbar. We conclude that the results are not significantly sensitive to this typical layer thickness estimate as the number of clusters and their positions along the S_P axis are generally consistent across the four values of ℓ, especially between $S_P \approx 34.18$ g/kg and $S_P \approx 34.62$ g/kg. We find the most reasonable clusterings occur when ℓ is chosen to be small enough that the features outside the pressure range we analyze do not significantly affect the moving average, yet large enough that the stair steps are completely smoothed out.

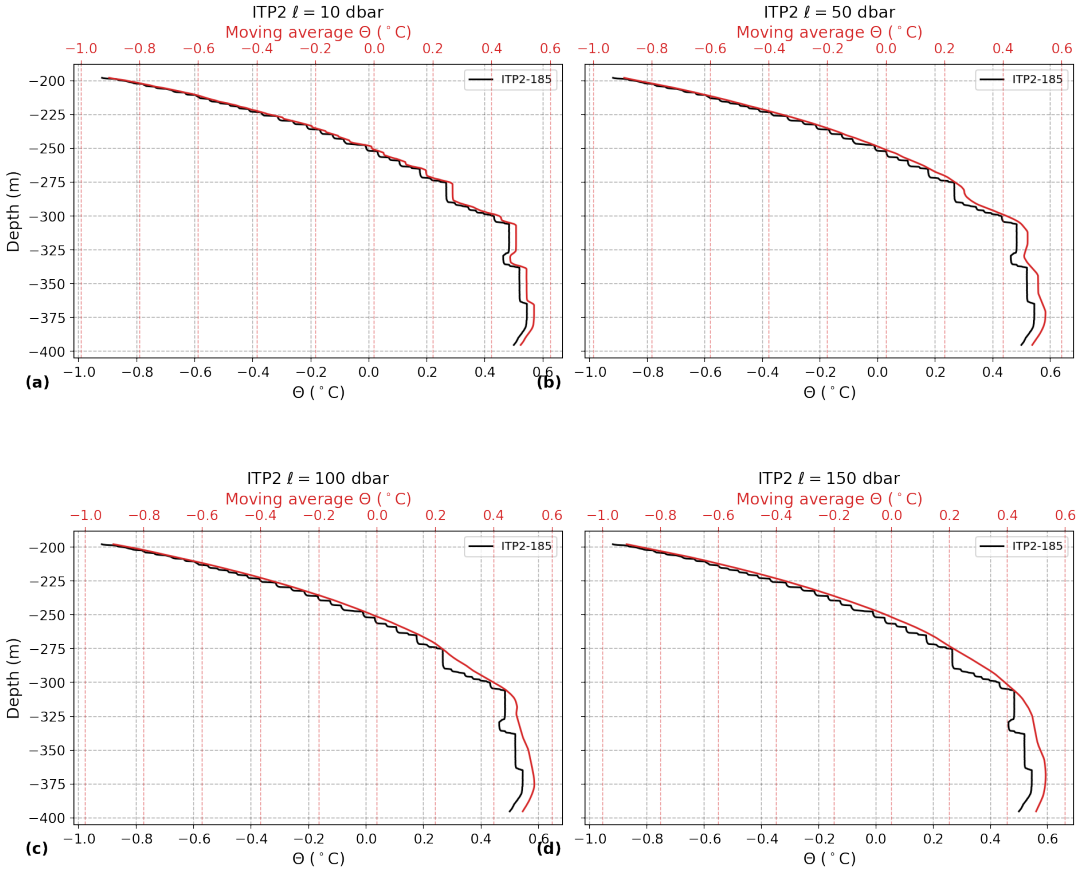

Figure S.3. *The original profile 185 from ITP2 and the smoothed version of that profile for 4 different values of ℓ: (a) 10 dbar, (b) 50 dbar, (c) 100 dbar, and (d) 150 dbar. The* Θ *axes on each panel are offset slightly to show both lines.*

S.3. Optional parameters for HDBSCAN

While m_{pts} has the most significant effect on the clustering results, there are several other parameters which could be adjusted when using the "hdbscan" Python package. In each case, we chose to follow the recommendation of the authors of the algorithm [3, 23]. The default distance metric is Euclidean and, as we cluster in a two dimensional space of continuous numerical variables, we maintain this selection. For the cluster selection method, we chose Leaf over Excess of Mass to avoid the results collapsing into fewer, larger clusters. HDBSCAN can be combined with DBSCAN by setting a threshold of cluster selection $\varepsilon_{clSelect}$ to explicitly group clusters a certain distance apart. However, we chose the default behavior of HDBSCAN which automatically identifies the values of ε which give the most stable clusters. HDBSCAN considers a neighborhood to be dense when m_{pts} points are within a certain distance ε. While m_{pts}, known as the minimum samples, can be independently set higher to more liberally include fringe points in clusters or lower to more conservatively classify them as noise, we follow the default recommendation to set this equal to the minimum points per cluster m_{clSize}.

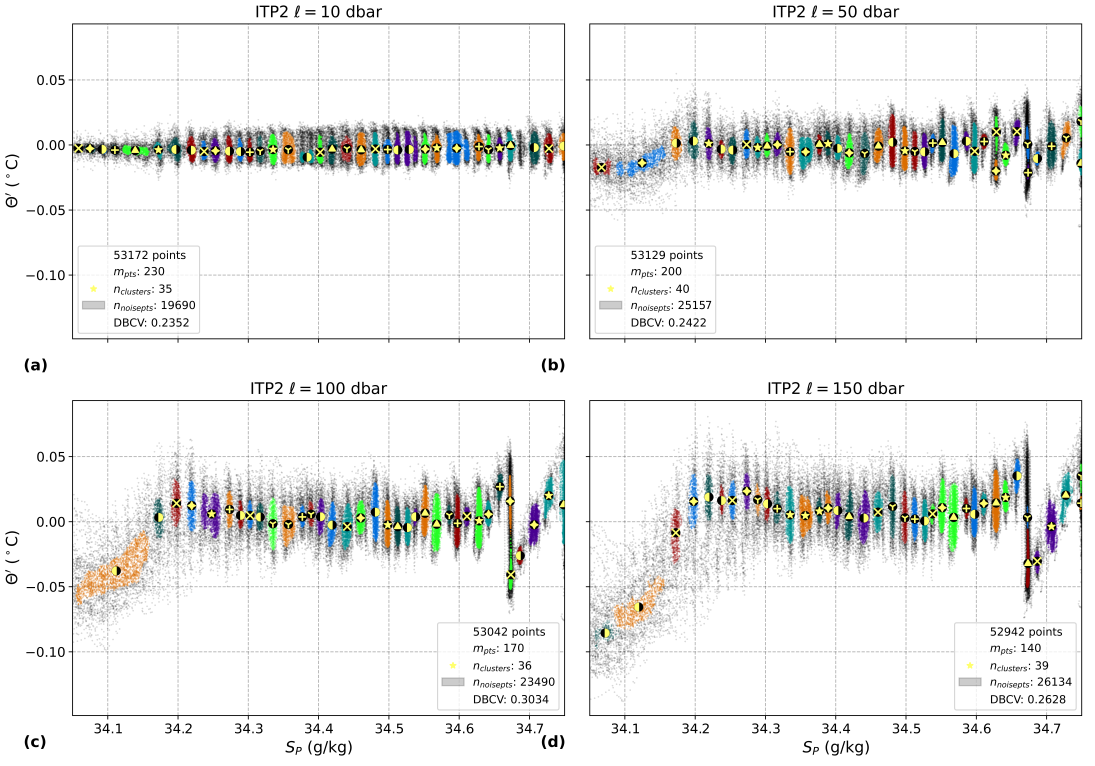

Figure S.4. *Clustered data from ITP2 in the salinity range 34.05—34.75 g/kg plotted in* Θ'*–*S_P *space for 4 different values of* ℓ*: (a) 10 dbar, (b) 50 dbar, (c) 100 dbar (the same as in Figure 2(c)), and (d) 150 dbar, where the gray points are noise and each color-marker combination indicates a cluster.*

S.4. Clusters from ITP3

In Figure S.5, we create a figure similar to that of Figure 2, but for ITP3. In Figure S.6, we create a figure similar to that of Figure 3(a), but for ITP3. Note that the run with $m_{pts} = 710$ had a DBCV score of 0.3885, which is slightly higher than the run at $m_{pts} = 580$ with a DBCV score of 0.3862. However, because the differences in DBCV were not great, we decided to use $m_{pts} = 580$ to reduce computation time as the clustering algorithm takes longer to run with higher values of m_{pts}.

S.5. Clusters across time for ITP2

In Figure S.7, we create a figure similar to that of Figure 4, but for ITP2.

S.6. Differences from T08

Figure 6 from Timmermans et al. [44] shows clusters in $\alpha\Theta - \beta S_P$ space with panel (a) showing five values of R_L for ITP2, which range from -3.5 to -3.0, and panel (b) showing 12 values of R_L for ITP5, which range from -3.9 to -2.4. It is unclear whether their reported $R_L = -3.7 \pm 0.9$ applies to data from ITP2, ITP5, both, or all six ITPs they included in their study. It is not explicitly stated whether that value applies to just the clusters shown in that figure or it includes the dozens of clusters they identified earlier in their study. T08 never explicitly state that they did not find a trend in R_L with respect to depth. However, given that T08 reported one overall value of R_L and that Bebieva and Timmermans [2] (which

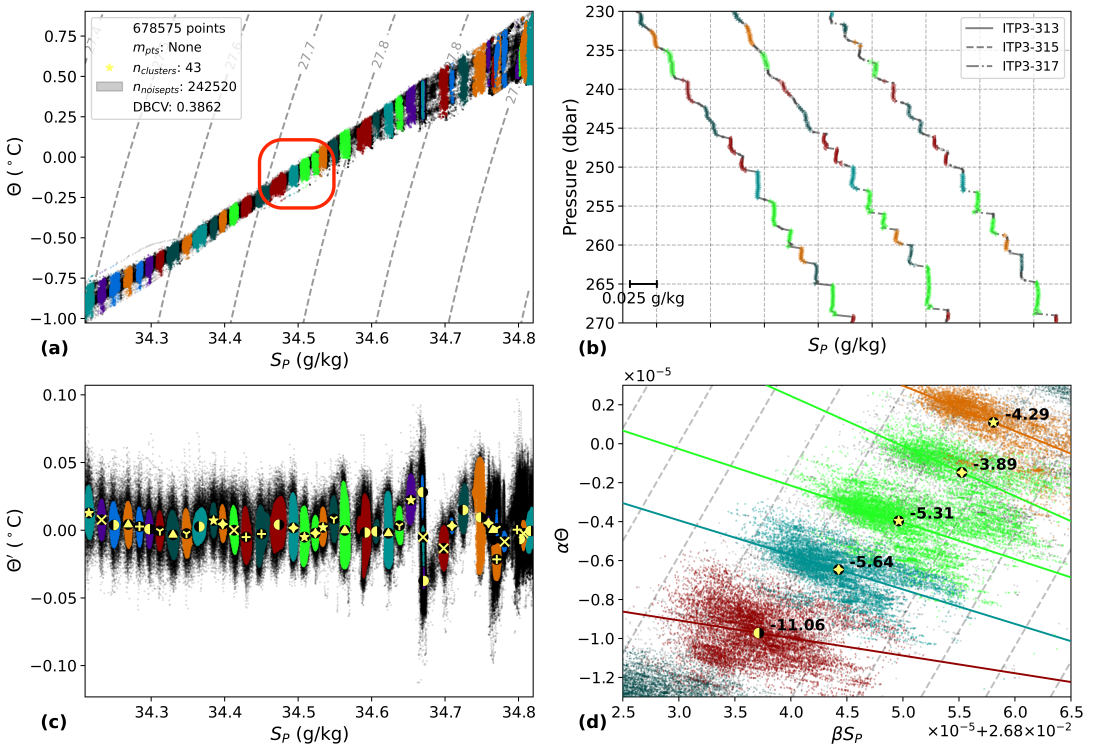

Figure S.5. *Results from the clustering algorithm with $m_{pts} = 580$ and $\ell = 100$ dbar run on 678575 data points in the S_P range 34.21–34.82 g/kg from all up-going ITP3 profiles. (a) The data in Θ–S_P space with dashed lines of constant potential density anomaly (kg m^{-3}) referenced to the surface. (b) Profiles 313, 315, and 317 from ITP3 in a limited pressure range to show detail. Each profile is offset in S_P for clarity. (c) The spatial arrangement used as input for the algorithm where the gray points are noise and each color-marker combination indicates a cluster. The same color-marker combinations are used in each panel and the markers in panels (c) and (d) are at the cluster average for each axis. (d) A subset of the data in αΘ–$βS_P$ space with the linear regression line and inverse slope (R_L) noted for each individual cluster and with dashed lines of slope $αΘ/βS_A = 1$.*

extended the work of T08) show a constant value of R_L in the depth range we consider, we assume T08 also found a constant value of R_L.

There are several factors that could explain why our results for R_L differ from those of T08. The fact that they used potential temperature θ while we worked with conservative temperature Θ is not relevant, since when we repeat our calculations using θ instead of Θ, the values of R_L we find are negligibly different. It is unclear whether T08 calculated the values of α and β for each point or for each layer. We calculated α and β for each point in each profile individually using functions from the Gibbs Seawater (GSW) Oceanographic Toolbox, the Python implementation of TEOS-10 [20], while T08 used the **?**] algorithm coded by **?**] as GSW was not yet released. This difference in the calculation of α and β may conceivably explain why the clusters we show in Figure 2(d) are tilted several degrees compared to those shown in Figure 6(a) from T08, and why the values of R_L found here are all less negative than corresponding values in Figure 6(a) of T08. The difference in calculating α and β may also account for the shift in the ranges of βS_P between the two figures. Both plots show a span in βS_P of 4.0×10^{-5}, but our plot ranges from 2.6838×10^{-2} to 2.6878×10^{-2}, while theirs ranges from 2.7002×10^{-2} to 2.7042×10^{-2}. Because the clustering algorithm only considers Θ′ and S_P, any difference in calculating α and β would not affect the clusters we found, only the values of R_L.

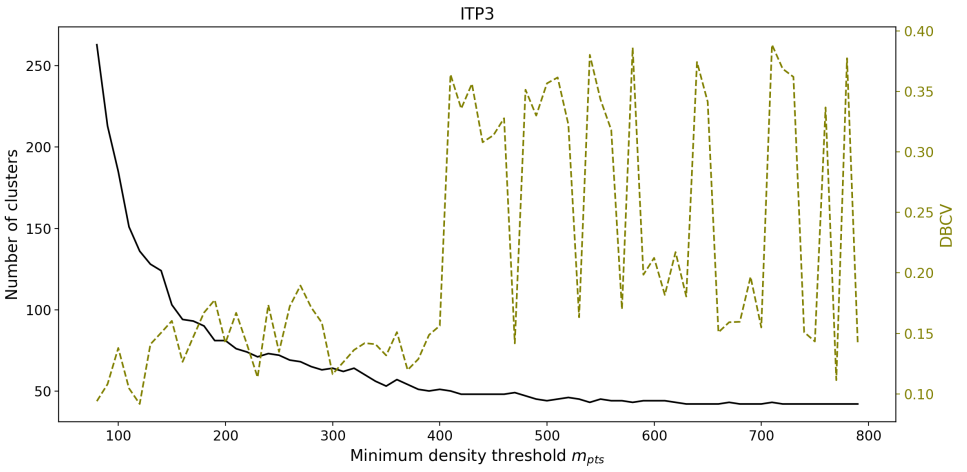

Figure S.6. *A parameter sweep showing the number of clusters found (solid lines) and DBCV (dashed lines) in ITP3 as a function of 72 different values of m_{pts} with $\ell = 100$ dbar.*

S.7. Differences from L22

L22 used 758 profiles from ITP3 while we used all 766 available up-going profiles. The reasons 8 profiles were not used was not stated, nor could we determine exactly which profiles they are. Based on the gaps in Figure 3 of L22, we believe that the 8 missing up-going profiles are from July 2006. We do not, however, believe that this difference of 8 profiles accounts in any significant way for the differences between our results and those of L22.

Instead, we believe the reason our results differ from those of L22 has to do with the difference in the methods used to identify layers. Because the method used by L22 to delineate different layers only considered salinity, they would not separate layers with temperature inversions. Remnant intrusions are homogeneous in salinity but, compared to stair steps, are inverted in temperature and have different patterns of heat and salt flux. They tend to be present near the bottom of the staircase, which is indeed where we find the largest differences between our results and those of L22. A remnant intrusion's pattern of a section of warmer water above a section of colder water is distinct enough for the clustering algorithm to find two clusters. However, if only salinity is considered, as L22 did, it would appear to be one regular staircase layer. Whether a remnant intrusion represents one or multiple layers is subjective, and we do not claim that one method is superior to the other. Here, in fact, it is the disagreement between these two methods is arguably the most interesting point, because it indicates that a specific physical process is operating.

While we agree with L22 that salinity is the best measured quantity by which to identify the layers of a staircase, it is still important to consider temperature. Another topic of future study would be to adapt this method to automatically distinguish between well-mixed layers and intrusions.

References

[2] Bebieva, Y. & Timmermans, M. L. (2019). Double-Diffusive Layering in the Canada Basin: An Explanation of Along-Layer Temperature and Salinity Gradients. *Journal of Geophysical Research: Oceans*, *124*(1), 723–735, https://doi.org/10.1029/2018JC014368.

[3] Campello, R. J. G. B., Moulavi, D., & Sander, J. (2013). Density-Based Clustering Based on Hierarchical Density Estimates. *Lecture Notes in Computer Science*, *7819*, 160–172, https://doi.org/10.1007/978-3-642-37456-2_14.

[] IOC, SCOR, & IAPSO (2010). The international thermodynamic equation of seawater – 2010 : Calculation and use of thermodynamic properties, volume 56. UNESCO.

[] McDougall, T. J. (1987). Neutral Surfaces. *Journal of Physical Oceanography*, *17*(11), 1950–1964, https://doi.org/10.1175/1520-0485(1987)017<1950:ns>2.0.co;2.

[20] McDougall, T. J. & Barker, P. M. (2011). Getting started with TEOS-10 and the Gibbs Seawater (GSW) Oceanographic Toolbox. 3.06.12 edition www.TEOS-10.org.

[] Morgan, P. P. (1994). SEAWATER: A Library of MATLAB® Computational Routines for the Properties of Sea Water: Version 1.2. Technical report, CSIRO Marine Laboratories, Hobart, Tasmania http://hdl.handle.net/102.100.100/239771?index=1.

[23] Moulavi, D., Jaskowiak, P. A., Campello, R. J. G. B., Zimek, A., & Sander, J. (2014). Density-Based Clustering Validation. In *Proceedings of the 2014 SIAM International Conference on Data Mining*, volume 2 (pp. 839–847). Philadelphia, PA: Society for Industrial and Applied Mathematics https://epubs.siam.org/doi/10.1137/1.9781611973440.96.

[44] Timmermans, M.-L., Toole, J., Krishfield, R., & Winsor, P. (2008). Ice-Tethered Profiler observations of the double-diffusive staircase in the Canada Basin thermocline. *Journal of Geophysical Research*, *113*, 1–10, https://doi.org/10.1029/2008jc004829.

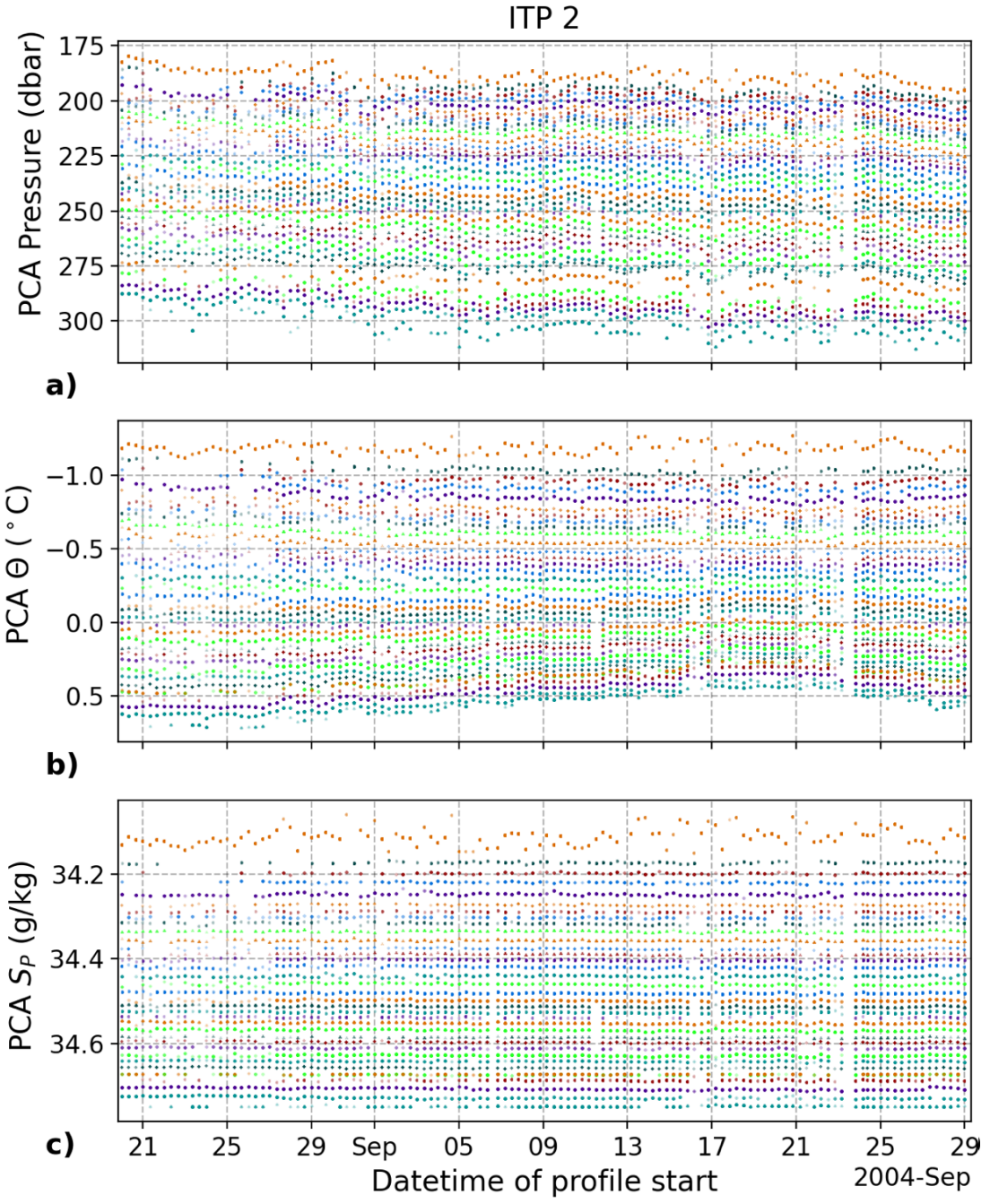

Figure S.7. *The average (a) pressure, (b) Θ, and (c) S_P for the points within each cluster for each profile (profile cluster average, PCA) across time. The clustering algorithm was run with m_{pts} = 170 and ℓ = 100 dbar on 53042 data points in the salinity range 34.05–34.75 g/kg from all up-going ITP2 profiles.*